RESEARCH ARTICLE-CHEMICAL ENGINEERING

A Numerical Optimization Approach for Removal of Astrazon Pink FG from Aqueous Media by Fenton Oxidation

Ayse Ozguven[1] · Dilara Ozturk[1]

Abstract

In this study, the treatment of aqueous media containing Astrazon Pink FG (AFG) dye, widely used in the textile industry but with limited studies, was investigated using the Fenton process. The system was numerically optimized as Fe^{2+}: 50 mg/L, H_2O_2: 50 mg/L, pH 3.75, reaction time: 42.54 min, and initial dye concentration: 100 mg/L based on the principle of low-cost high removal efficiency. The quadratic model with central composite design was reliable, valid, and significant ($p < 0.0001$) for both system responses Theoretical removal efficiencies under these conditions were determined as 80.5% and 94.11% for chemical oxygen demand (COD) and AFG removal, respectively, and were confirmed experimentally as 81.01% and 94.33% under the same conditions. The performance of the Fenton process under optimized conditions was calculated as 51%, 65%, and 73% for COD, AFG and Methyl Orange removal. Reactive Yellow 86, Acid Orange 7, and Reactive Green 19 were removed as 62.72%, 51.73%, and 39.39%, respectively, from real textile wastewater. The generated sludges (v/v) under optimized conditions for AFG dye solution, binary dye solution and real textile wastewater were 6%, 5% and 7%, respectively. AFG removal best fitted the BMG model ($R^2 > 0.998$). According to the experimental cost estimation based on chemical consumption under optimized conditions, 1 m^3 of AFG solution can be treated at \$0.26. It was concluded that the Fenton process could be used as a pretreatment for industrial wastewater containing dye.

Keywords Dye · Fenton · Optimization · Oxidation

1 Introduction

Depending on developing technology and changing human needs, industries have increased their product range and diversity in many areas. Dyes are one of the raw materials used to respond to this diversity in all kinds of colored things and consumables, as well as in the medical sector. However, today, the textile industry, commercial dye production industry, and food sector have a large share in the use of dyes. Approximately 2% of dyes produced every year in the world are mixed into wastewater as a result of production activities, while the majority of dyes, 10%, are discharged from industries such as the textile industry, highlighting the magnitude of dye pollution discharged from the industry[1, 2]. When these wastewaters are discharged into the receiving environment without treatment, they disrupt the oxygen balance of the environment, reduce light transmittance, and put the living organisms at risk [3]. In addition, the discharge of this wastewater to receiving environments causes problems such as eutrophication. It endangers human and animal life by entering the food chain through the usual ecosystem cycle. Although there are major risk environments for wastewater, dyes containing toxic and carcinogenic active substances are risky for human life. In every respect, the treatment of these wastewaters is essential.

According to their chemical structures, dyes are divided into classes such as azo, nitro, and reactive. AFG is a cationic dye frequently used for dyeing wool, silk, leather, and fiber. Many studies have investigated the effectiveness of aerobic, anaerobic, adsorption, and advanced oxidation processes for the treatment of solutions containing dyes [4–6]. Krishnan et al. [7] investigated the removal of Reactive Brilliant Red X-3B (RBRX-3B), Direct Blue-6 (DB-6), and Direct Black-19 (DB-19) dyestuffs under aerobic conditions. Maximum removals of RBRX-3B, DB-6, and DB-19 were 31.2%, 71.5%, and 87.6%, respectively. Although effective yields

✉ Dilara Ozturk
dozturk@yyu.edu.tr

1 Department of Environmental Engineering, Faculty of Engineering, Van Yuzuncu Yil University, Van, Turkey

Springer

are obtained in aerobic processes, hydraulic retention time requirements, large space requirements, and a large amount of sludge formation can be counted among the disadvantages of this system [8, 9]. Dye removal with advanced oxidation processes is a very successful and popular method.

The advanced oxidation processes (AOP) are based on the production of oxidative radicals as a result of a series of chemical and physical processes, and these radicals attack organic materials and break them down to intermediate or end products [10]. Hussain et al. [11] reported that the O_2^-, HO_2, OH radicals, and H_2O_2 play an essential role in AOP on the degradation of dyes.

Ozturk and Yilmaz [12] investigated the removal of Basic Red 13 (BR13) dye from aqueous environments with an electrochemical oxidation method. COD removal of 99.98% was achieved, and 7.91 kWh/m^3 energy consumption was required. Although there was no secondary waste generation such as sludge, high energy consumption and expensive inert electrodes limit the system.

A study that investigated the AFG degradation mechanism by glow discharge electrolysis (GDE) technique was made by Quanfang et al. [13]. GDE is an electrolysis technique applied with several hundred volts [14]. OH, H, and O radicals can be formed to oxidize the organics in this process like the anodic oxidation process. The total organic carbon (TOC) removal and decolorization were 72.6% and 99.0% under 600 V discharge voltage for 120 min reaction time. However, electrolysis, electrooxidation, electrocoagulation, electro-Fenton processes, etc., have high removal efficiencies of pollutants. So, their applications may not be economical due to electricity use.

The Fenton process is an AOP application in which hydroxyl radicals are produced in the presence of ferrous ion and hydrogen peroxide in an aqueous medium. It is possible to convert pollutants into end products such as H_2O and CO_2 with hydroxyl radicals [15]. It is also chosen as a pretreatment process in which highly resistant pollutants are converted into intermediate products. The Fenton process has some disadvantages; external chemicals such as H_2O_2 constitute a large part of the operating cost [16], and sludge production after the reaction. However, Fenton processes are preferred due to the system's ease of operation, high pollutant removal efficiencies, and rapid results. Many studies reported high removal efficiencies for dye-containing wastewaters with Fenton and Fenton-like processes [17, 18]. The nanomaterials were frequently used for the removal of dyes with photocatalytic systems [19, 20] and heterogeneous Fenton (or Fenton-like) processes [21]. Mahmud et al. [22] used $Fe_3O_4@SiO_2$ nanocatalyst to degrade malachite green with a heterogeneous Fenton-like process. They reported 96.18% removal of malachite green with magnetically separable catalyst. Modarresi-Motlagh et al. [23] investigated crystal violet (CV) removal with Fenton-like oxidation, and

they reported 90–100% CV removal in a continuous stirred tank reactor. Tabai et al. [24] reported 100% degradation of Acid Orange 7 with a homogeneous Fenton-like system based on hydrogen peroxide and a recyclable Dawson-type heteropolyanion. Modak et al. [25] investigated the efficiency of a rotating packed bed reactor for methyl orange decolorization with a homogenous Fenton process. They stated over 90% methyl orange removal. As seen, the Fenton and Fenton-like processes are successful for treatment of dye-containing aqueous medias.

The efficiency of one process depends on the characteristics of the wastewater [26] and the optimization success of the system. Optimization can be summarized as improving the conditions in the most economical way to get the best results. As an engineering practice, there are many methods to optimize systems. Nowadays, it is possible to optimize systems with programs that often combine statistical and mathematical methods or artificial intelligence applications. Response surface methodology (RSM) is one of the statistical-mathematical optimization programs. RSM provides a significant advantage in terms of economy, which is one of the most critical issues of the optimization process, with a minimum number of consumables, time, and labor on a laboratory scale [27].

There are a limited number of studies in the literature about AFG removal, which is frequently used in acrylic fiber and knitted fabrics and with a need for investigation of removal from wastewaters.

As far as the authors are aware, there is no study investigating AFG removal with the Fenton process optimizing the operating conditions using RSM. The decolorization kinetics were investigated to understand the oxidation mechanism better. The high removal efficiency and economical application of the Fenton process in this study highlight the significance of the numerical optimization approach. The findings will contribute to a better understanding of the oxidation mechanism of dye-containing wastewaters and optimization of the Fenton process to treat wastewater containing AFG.

2 Material and Method

2.1 Preparation of Dye Solutions and Chemicals

AFG ($C_{22}H_{26}Cl_2N_2$) and methyl orange ($C_{14}H_{14}N_3NaO_3S$) were commercially purchased from Tokyo Chemical Industry (product number: A0867, purity:99%) and Sigma-Aldrich (USA) (CAS number: 547-58-0, purity: 99%). Concentrations varying from 100 to 500 mg/L were prepared from a stock solution of 1000 mg/L. 0.02 N NaOH (CAS number: 1310-73-2, purity: $\geq$ 98%) and 0.02 N HCl (CAS number: 7647-01-0, purity: 37%) were purchased from

Table 1 Characterization of dye solutions and textile wastewater

Parameter	AFG Solution (100 mg/L)	Binary Dye Solution (50 mg/L Methyl Orange and AFG)	Real Textile Wastewater
pH	3.75	4.70	7.7
Dissolved Oxygen (DO, mg/L)	1.1	1.4	0.7
EC	70 (μs/cm)	44 (μs/cm)	5.13 (mS/cm)
Total Dissolved Solid (TDS, mg/L)	32.5	18.5	2520
Total Suspended Solid (TSS, mg/L)	2.5	5	1685
COD (mg/L)	763.8	748.9	1700
Total Nitrogen (TN, mg/L)	8.08	10.15	20.36
Solubility in Water (g/L)	14	5	–
Temperature (°C)	20 ± 5	20 ± 5	16 ± 5

Sigma-Aldrich and used to set pH values of dye solutions. H_2O_2 (CAS No: 7722-84-1, purity: 30%) and $FeSO_4.7H_2O$ (CAS number: 7782-63-0, purity: $\geq$ 99%) were provided from Sigma-Aldrich (USA). Binary dye solutions containing 50 mg/L methyl orange and AFG were prepared to investigate the process efficiency under mixed dye media. Also, real wastewater is provided from a textile industry in Malatya, Turkey. Characterization of dye solutions and wastewater is given in Table 1.

2.2 Experimental Procedure

The Fenton experiments focused on removing COD from various aqueous media. The first of these is aqueous solutions containing only AFG. Since this study focused on the removal of AFG dye, the optimization of the experimental system was carried out only for operational conditions where COD removal from AFG-containing solutions was investigated. The second contaminant medium is the binary dye solution. The binary dye solution contains a mixture of AFG and methyl orange dye at certain concentrations (50 mg/L). The removals of AFG and methyl orange dye from binary solution under optimized conditions are discussed. In this experimental system, the aim is to demonstrate AFG removal under conditions optimized for AFG in the presence of any dye. Finally, COD and particular dye removal efficiencies were investigated under optimized conditions for real textile industry wastewater in Malatya, Turkey. The operating parameters for each experimental system are ferrous ion concentration (50–300 mg/L), H_2O_2 concentration (50–600 mg/L), pH of the solution (2.5–5.0), reaction time (15–60 min), and initial AFG concentration (C_0, 100–500 mg/L). All operating parameters were adjusted to desired values for 500 mL aqueous mediums. The pH was adjusted to the desired value using 0.02 N HCl or 0.02 N

NaOH. After the pH adjustment, Fe^{2+} ions were added and mixed in the first stage, and H_2O_2 was added in appropriate doses in the second stage. After the addition of Fe^{2+} ions and H_2O_2, the reaction was started by mixing the solutions in the Jartest device (Velp Scientifica, JLTA, Italy) at 150 rpm for 60 min. At the end of the reaction, the pH value of the solution was set to 7 for the iron sludge precipitation for 30 min[28]. Then, 20 mL of supernatant phase is taken from this solution and centrifuged at 8000 rpm. The remaining concentrations of H_2O_2 and COD in the aqueous solutions after centrifugation were determined. In addition, the amount of sludge formed for all three test systems under optimized conditions was calculated. Analyzing methods are given in Sect. 2.3

2.3 Analyzing Methods

System efficiency was calculated for both COD and dye removal. The well-known Eq. 1 was used to calculate COD and dye removal efficiencies. While C_0 refers to the solutions' initial COD and dye concentration (mg/L), C_t refers to the COD and dye concentration in wastewater samples taken at time t. AFG and methyl orange removal efficiencies were analyzed at a wavelength of 522 nm and 462 nm, respectively. The UV–Vis scan of AFG, methyl orange, and binary dye solutions are shown in Fig. S1.

$$\text{Removal efficiency (\%)} = \frac{(C_0 - C_t)}{C_0} \times 100 \tag{1}$$

pH was analyzed with a multimeter (WTWmulti340i). Dissolved oxygen (DO) and temperature of solutions were analyzed with a multimeter (YSI 556 MPS). A jar test machine was used for batch experiments (Velp JL T6). All experiments were conducted with 150 rpm of stirring speed. A UV–Vis spectroscope (WTW photolab 6100 vis) was used

to determine the COD and AFG concentrations in solutions taken at different time intervals. COD analysis was conducted according to the closed reflux colorimetric method [29], and AFG analysis was determined at a wavelength of 522 nm. Total nitrogen (TN) analysis was made a cell test method (based on peroxydisulfate oxidation/2,6-dimethylphenol) by using a spectrophotometer (WTW photolab 6100 vis) at a wavelength of 320 nm. The H_2O_2 concentrations remaining in the solution after the reaction [30] were quickly read due to possible COD interference according to the method determined by Talinli and Anderson [31] and Benatti et al. [32].

Total dissolved solids (TDS) is an important parameter that shows the measure of all inorganic and organic substances found in mineral, ionized, and dissolved forms in solution [33, 34]. TDS in a water sample can be measured gravimetrically in ppm (parts per million) or mg/L [35]. In this study, TDS analyses were made according to the Standard Methods for the Examination of Water and Wastewater [36]. Briefly, 150 mL of glass beakers was dried in an oven for 24 h at 180 °C. The dried glass beakers were cooled for 2 h in a desiccator and then weighed; 100 mL of samples was filtered with 0.45-μm cellulose acetate membrane (Product No: 10404006, Whatman Int. Ltd., UK). The filtered samples were transferred to the glass beaker. Then samples were evaporated in an oven for 24 h at 180 °C. The dried and cooled glass beakers were weighed again to calculate TDS concentration. TSS analyses were made according to the Standard Methods for the Examination of Water and Wastewater [36] based on the gravimetric method. Under vacuum, the 100 mL of samples was filtered with a 1.2-μm filter (Cat No: 1822–047, Whatman Int. Ltd., UK). Then filter papers were dried in an oven for 24 h at 103 °C before filtering the samples to provide the constant weight. After the filtering process, the filter papers were dried in an oven for 2 h at 103 °C. The dried and cooled filters were weighed again to calculate TSS concentration. All analyzes were performed in triplicate.

2.4 Calculation of Fenton Sludge

The sludge formation was analyzed for three experiment sets. One and second sets were conducted under the optimized conditions for aqueous solutions containing only AFG dye and for binary dye solutions. The last set was conducted under optimized conditions for real textile wastewater. At the end of these experiments, the pH values of solutions were set as 7.0 to provide precipitation of iron. After this procedure, the solution was filtered under vacuum using a 0.7-μm filter (Cat No: 1825-047, Whatman Int. Ltd., UK). Then the filter paper was dried in an oven (Memmert UN 110) for 1 h, and the weight of dried sludge was measured [37].

2.5 Optimization Pathway

Optimization is frequently used in engineering to obtain maximum output from a system within certain constraints. It can be summarized as optimizing system conditions to operate a system with most efficiency. Today, optimization can be achieved with many statistical and mathematical programs. Design expert 13® is a software package from Stat-Ease Inc. that includes many optimization procedures such as Box–Behnken, central composite design for response surface applications. Also, it includes Plackett–Burman and Taguchi designs under factorial designs, and other custom and composite design models. Optimizing more than one variable for one or more responses, determining the individual, interaction and quadratic effects and effect levels of each variable or variables on the response/s, statistical analysis of the data and the established models, optimizing the parameters by adjusting them in the desired ranges, estimating data without experiment from model equations (within parameter limits), and determining the reliability level of this estimation are possible with the Design expert 13® software. Design expert 13® offers numerical and graphical optimization options for models with the program, and the experimenter can determine the optimum points by performing the optimization using the matrix method [27].

RSM examines the relationship between system inputs and output variables based on factorial contributions from coefficients using a regressive model [38] and meets expectations in many aspects in an optimization procedure. Central composite design (CCD) was used to optimize the system as a response surface application in this study. An experimental system is optimized while ensuring economy with minimum chemical consumption, time spent, and labor, along with maximum system efficiency. In addition, determining the most critical parameters affecting the system, fixing the parameters that do not have much effect on the system, narrowing the intervals of the optimization parameters, and approximating the optimum response are possible with the analysis of variance (ANOVA) test. It is possible to determine to what extent the change of 1 unit in each operating parameter affects the system output or outputs with the p-value using the ANOVA test. In addition, the reliability and adequacy of the model can be determined in the specified space [39]. One of the essential advantages of RSM is predicting the results without experimenting with the specified parameter ranges and reaction environment. It is possible to analyze how close these estimated values in the RSM space are to the experimental data for each optimization procedure. With RSM, a quadratic equation including the effects of individual, interaction, and quadratic effects of system inputs on system output or outputs is obtained (Eq. 2) [40] with the

Table 2 Range of independent parameters

Parameter	Minimum Point (−1)	Center Point (0)	Maximum Point (+ 1)
A	50	175	300
B	50	325	600
C	2.5	3.75	5
D	15	37.5	60
E	100	300	500

$$\hat{y}_n = \beta_0 + \sum_{i=1}^{n} \beta_i x_i + \sum_{i=1}^{n} \beta_{ii} x_i^2 + \sum_{i=1}^{n} \sum_{J=i+1}^{n} \beta_{ij} x_i x_j + \varepsilon \quad (2)$$

While x_i symbolizes the level of independent input, β_i, β_{ij} and β_{ii} represent the linear, interaction, and quadratic effect of terms, β_0 ε is the constant response value representing the random error, and n is the number of independent factors. There are three design points in CCD [41]. These are fractional factorial, center, and axis points [3]. The number of experiments in CCD can be determined by Eq. 3 [42].

$$2^k + 2k + c \quad (3)$$

Here, c stands for the number of repeated experiments in the center (8 in this study), and k is the number of independent variables in the system (5 in this study). There are three types of design points in CCD. Independent variables were selected as ferrous ion concentration (mg/L) (coded as A), H_2O_2 concentration (mg/L) (coded as B), pH of solution (coded as C), reaction time (min) (coded as D), and initial AFG concentration (C_0, mg/L) (coded as E). The maximum, minimum, and center points for these variables are given in Table 2.

Optimization with CCD in RSM can be performed by various methods such as graphical [43], matrix [27], and numerical [41]. With the numerical optimization method, the best values for inputs and outputs in the design space are offered to the experimenter with desirability levels. One of the most critical issues in numerical optimization is determining the input and output targets. All independent parameters were targeted as 'in range' except for ferrous ion concentration and H_2O_2 concentration in this study. Ferrous ion concentration and H_2O_2 concentration factors were targeted as 'minimize' to reduce the excessive use of chemicals for an economical approach. Both output parameters were targeted as 'maximize.' Then, the most suitable solution was selected according to the desirability values.

3 Results

3.1 CCD Matrix, Regression Analysis, and Model Analysis

The experimental matrix designed by RSM, both experimental and predicted results, is shown in Table 3. The effects of the five coded parameters on removal (%) of COD and AFG defined as system outputs were investigated. As a result of 50 experimental sets, the coded model equations for both outputs are shown in Eqs. 4 and 5. With the help of these equations, it is possible to estimate the outputs by entering the inputs within the value ranges introduced to the system. The accuracy of this estimation is examined with both experimental and model validation analyses. Table 3 shows the corresponded error (ε) values that can be calculated the differences between experimental and predicted values for both responses. As seen from Table 3, predicted values are generally close to experimental values, which can be interpreted as established model success for predicting the actual values. The model reliability can be more interpreted with ANOVA tests (see Table 6).

The maximum results were obtained for COD removal and AFG removal in the experimental set in run 39 (Table 3). This can give the experimenter insight into estimating the optimum points of each parameter [41]. At the same time, it is possible to estimate ranges of values close to the optimum point from 3D plots (see Figs. 2 and 3). The relationship between system outputs and inputs was explored with the empirical coded model given in Eqs. 4 and 5. The positive and negative values indicate the synergistic and antagonist effects between system outputs and inputs, respectively [44]. For both system outputs, the effects of individual factors are synergistic, except for the initial AFG concentration, while the effects of all quadratic parameters are antagonistic. The interaction effects of the parameters exhibited both synergistic and antagonistic properties.

COD Removal (%)(**Coded**)

$$= 91.72 + 8.88[\mathbf{A}] + 11.24[\mathbf{B}] + 6.40[\mathbf{C}]$$
$$+ 5.13[\mathbf{D}] - 9.24[\mathbf{E}] + 5.07[\mathbf{AB}]$$
$$- 3.18[\mathbf{AC}] - 0.40[\mathbf{AD}] - 0.37[\mathbf{AE}] + 1.70[\mathbf{BC}]$$
$$- 0.61[\mathbf{BD}] + 2.11[\mathbf{BE}] - 1.31[\mathbf{CD}]$$
$$+ 1.26[\mathbf{CE}] + 0.12[\mathbf{DE}] - 3.84[\mathbf{A}]^2 - 1.278[\mathbf{B}]^2$$
$$- 7.12[\mathbf{C}]^2 - 3.63[\mathbf{D}]^2 - 1.66[\mathbf{E}]^2 \quad (4)$$

AFG Removal (%)(**Coded**)

$$= 98.38 + 4.82[\mathbf{A}] + 6.37[\mathbf{B}] + 4.16[\mathbf{C}] + 4.03[\mathbf{D}]$$
$$- 7.92[\mathbf{E}] + 3.33[\mathbf{AB}] - 2.91[\mathbf{AC}]$$
$$- 3.39[\mathbf{AD}]] + 2.25[\mathbf{AE}] + 2.14[\mathbf{BC}] + 2.47[\mathbf{BD}]$$

Table 3 CCD matrix and experimental results

Run	A	B	C	D	E	COD Removal (%) Experimental	COD Removal (%) Predicted	AFG Removal (%) Experimental	AFG Removal (%) Predicted
1	300	50	5	15	500	35.12	34.16	72	70.99
2	300	600	2.5	60	500	80.56	79.75	91.51	90.75
3	50	600	5	15	500	62.28	62.05	78.12	77
4	175	325	3.75	60	300	97.95	97.22	99.68	98.78
5	175	50	3.75	37.5	300	80.99	80.69	92.74	92.28
6	175	325	3.75	37.5	300	87.77	89.72	93.84	93.38
7	300	600	2.5	15	100	83.75	83.42	94.4	93.28
8	50	50	2.5	15	100	40.05	41.67	80.1	79.99
9	300	325	3.75	37.5	300	96.54	96.76	99.83	100
10	300	50	2.5	60	100	65.43	64.26	81.72	81.2
11	50	50	5	60	500	33.76	34.74	65.25	65.18
12	300	600	5	15	500	68.95	67.65	89.45	90.88
13	300	600	5	15	100	90.18	89.38	98.8	97.36
14	50	325	3.75	37.5	300	80.99	79.9	97.74	96.26
15	175	325	3.75	37.5	300	88.52	89.72	95.32	94.38
16	175	325	3.75	15	300	80	81.96	94.52	93.01
17	50	600	2.5	15	500	20.57	20.34	51.33	52.92
18	50	600	2.5	60	100	58.53	57.82	89.73	88.38
19	175	325	3.75	37.5	300	94	92.72	98.99	98.38
20	50	50	2.5	60	500	27.41	26.09	57.25	55.61
21	50	50	2.5	15	500	18.14	9.94	44.86	45.2
22	175	325	5	37.5	300	78.5	77	99.52	98.91
23	50	50	5	60	100	63.62	62.94	92.24	91.35
24	50	50	5	15	500	22.37	23.84	55.42	56.99
25	175	325	3.75	37.5	100	97.58	99.3	99.78	100
26	300	50	5	60	100	58.99	57.15	84.99	81.77
27	175	325	3.75	37.5	300	96.44	95.72	99.52	98.38
28	300	600	2.5	15	500	57.34	57.65	79.6	80.78
29	300	50	2.5	60	500	31.13	30.52	61.06	60.98
30	50	50	5	15	100	48.77	47.53	78.26	78.77
31	300	50	5	60	500	48.82	48.45	66.72	67.56
32	50	600	2.5	60	500	31.69	31.03	66.01	67.51
33	175	325	3.75	37.5	300	85.06	84.72	93.51	93.38
34	175	325	3.75	37.5	300	96.83	95.72	99.86	98.38
35	300	600	5	60	500	71.53	72.49	93.55	92.63
36	50	600	2.5	15	100	35	36.61	70.84	71.39
37	300	50	2.5	15	100	47.72	48.2	86.02	87.02
38	50	600	5	60	500	61	59.49	92.7	91.38
39	**175**	**600**	**3.75**	**37.5**	**300**	**98.66**	100	**99.97**	100
40	300	50	2.5	15	500	21.02	21.98	61.8	62.19
41	50	600	5	60	100	71	70.23	93.53	93.23
42	300	50	5	15	100	52.74	53.34	82.86	84.81
43	175	325	2.5	37.5	300	52.48	53.2	85.38	86.58

Table 3 (continued)

Run	A	B	C	D	E	COD Removal (%) Experimental	COD Removal (%) Predicted	AFG Removal (%) Experimental	AFG Removal (%) Predicted
44	50	600	5	15	100	60	61.28	78.64	80.46
45	175	325	3.75	37.5	500	84.31	82.82	92.34	91.44
46	300	600	2.5	60	100	83.29	84.03	95.2	95.64
47	300	600	5	60	100	88.82	89.73	98.73	98.51
48	175	325	3.75	37.5	300	88.06	88.72	95.77	96.38
49	175	325	3.75	37.5	300	90	90.72	96.58	98.38
50	50	50	2.5	60	100	44.75	44.33	82.38	82.79

$$+ 3.73[\mathbf{BE}] - 0.05[\mathbf{CD}] + 3.15[\mathbf{CE}]$$
$$+ 1.30[\mathbf{DE}] - 0.4[\mathbf{A}]^2 - 1.55\mathbf{B}^2$$
$$- 2.99[\mathbf{C}]^2 - 1.32[\mathbf{D}]^2 - 1.75[\mathbf{E}]^2 \tag{5}$$

Model summary statistics and the sequential model sum of squares tables for both responses are shown in Table 4 and Table 5, respectively. In Table 4, the 'quadratic' model is suggested for both responses, and the 'cubic' model is aliased. The fact that the *Adjusted R^2* and *Predicted R^2* values are close to each other is one of the most important factors in recommending a model. Accordingly, the 'cubic' model cannot be used for modeling data [41, 45]. In addition, it can be concluded that 'linear' and '2FI' models cannot be used to model experimental data. The F value is another parameter determining model selection. A large F value indicates the selectability of the model. In Table 5, the highest F value was obtained for the 'quadratic vs. 2FI' model in both responses. The *p*-value is a factor that is often used in determining the effectiveness of a model or parameter. It is clear from Table 4 that 99.99% effect was obtained for the 'quadratic vs. 2FI' model. When the *p*-value is analyzed for response 2, the 'Linear' model has 99.99% significance. However, it is not recommended by the system. 'Adjusted R^2,' 'Predicted R^2,' '*p*-value,' and F values should be evaluated together when deciding on the model. Therefore, the *p*-value obtained for the second response becomes insignificant when Table 4 is examined. This is because there is no R^2 consistency for the linear model; as a result, it can be concluded that the 'quadratic' model is valid for both system outputs.

The predicted vs. actual graphs are informative in verifying how successful the model is in predicting responses. Figure 1a and b shows predicted vs actual plots for responses 1 and 2. The closeness of the experimental and predicted data to the line reveals the model's success in predicting the data. The colored boxes above and below the line represent each experimental and predicted data, respectively. Experimental data are the actual values taken as responses (COD and AFG removal). Predicted values are the estimated COD

and AFG values from the established quadratic model with Eqs. 4 and 5. As can be seen, the experimental and predicted data are located close to each other around the line. Therefore, it can be concluded that the established quadratic model successfully predicts both responses in the working ranges. The relationship between the data estimated by the system and the level of residuals for response 1 and response 2 are given in Fig. 1c and d, respectively. The scattered colored boxes represent the result of the experimental sets and the estimated data for each response. Externally studentized residual plot helpful to evaluate the significance outlier of the points. In this evaluation, the outside red lines are defined as outlier points [46]. A residual is an error that is the difference between the predicted values (scatterplot) and the observed values (regression line) [46]. A distribution close to the zero axis indicates the closeness of the estimates to the experimental data, while it indicates that the residuals are minimal. As seen, the range of residual values between −3 and + 3 are within the acceptable limits [47], and the variance of observed values is constant [48]. Based on these data, it can be said that the variance of the actual values is constant, the input parameters in the model do not need to be transformed, and the established model is satisfactory and valid [49].

3.2 Effect of Independent Parameters on Responses

The most important indicator in determining the degree of influence of parameters affecting an experimental system in CCD is the ANOVA table (Table 6). As shown in Table 6, it is clear at $p < 0.0001$ that the model established for both responses is significant. The F values for the 1st and 2nd responses are 34.28 and 31.91, respectively. This situation indicates that the established quadratic regression is significant [41]. It is noteworthy that the effect significance of the system parameters for both responses is the same for the important parameters. The order of importance of the independent parameters for COD removal was H_2O_2 Conc. > Initial AFG Conc. > Fe Conc. > pH > time, while the order of significance for AFG removal was: Initial AFG Conc. >

Table 4 Model summary statistics for Response 1 and Response 2

	Source	SD	R^2	Adjusted R^2	Predicted R^2	Press	
Response 1	Linear	20.11	0.4061	0.3386	0.2711	21,846.87	
	2FI	21.89	0.4565	0.2167	−0.1038	33,082.52	
	Quadratic	**6.48**	**0.9594**	**0.9314**	**0.8574**	**4273.31**	**Suggested**
	Cubic	6.58	0.9798	0.9292	0.4747	15,745.77	Aliased
Response 2	Linear	11.07	0.4949	0.4375	0.3579	6850.66	
	2FI	10.98	0.6157	0.4462	0.1984	8552.14	
	Quadratic	**4.00**	**0.9565**	**0.9266**	**0.8524**	**1574.96**	**Suggested**
	Cubic	3.84	0.9807	0.9323	−0.1946	12,745.63	Aliased

Table 5 The sequential model sum of squares for response 1 and response 2

	Response 1					Response 2				
Source	Sum of Squares	df	Mean Square	F-value	*p*-value	Sum of Squares	df	Mean Square	F-value	*p*-value
Mean vs Total	2.124E + 05	1	2.124E + 05			3.612E + 05	1	3.612E + 05		
Linear vs Mean	12,171.34	5	2434.27	6.02	0.0003	5279.74	5	1055.95	8.62	< 0.0001
2FI vs Linear	1510.35	10	151.04	0.3152	0.9717	1289.21	10	128.92	1.07	0.4115
Quadratic vs 2FI	**15,074.56**	**5**	**3014.91**	**71.88**	**< 0.0001** Suggested	**3636.25**	**5**	**727.25**	**45.48**	**< 0.0001** Suggested
Cubic vs Quadratic	610.01	15	40.67	0.9390	0.5493 Aliased	257.53	15	17.17	1.17	0.3897 Aliased
Residual	606.35	14	43.31			206.22	14	14.73		
Total	2.424E + 05	50	4847.91			3.719E + 05	50	7438.24		

H_2O_2 Conc. > Fe Conc. > pH > time (Table 6, F-values). These results are confirmed by the perturbation plots displayed for both responses in Fig. S2. The perturbation plot is useful for comparing the effects of all factors at a given point in the design space. The midpoint of all factors (i.e., code 0) is set as the reference point (Fig. S2). As clear in Fig. S2(a), the main effective factor with high steepness for COD removal is B (H_2O_2 Conc.) while the main factor on AFG removal is E (Initial AFG Conc.) (Fig. S2b). COD and AFG removal efficiencies were less sensitive for reaction time. Also, Table 6 shows that system parameters 'individual' effects are significant for both responses with $p < 0.0001$. Values greater than 0.1000 indicate that the model terms are not meaningful, so it can be said that the 'interaction' and 'quadratic' effects of the parameters affect both responses less significantly compared to the individual effects (except CC for COD removal, BE for AFG removal). Additionally, Pareto analysis is very useful for testing the impact of parameters on response. Figure S3 shows the effect of terms and

their interactions with 95% confidence lines. The percentage effect of each term was calculated from Eq. (6) [42].

$$P_i = \left(\frac{\beta_i^2}{\sum \beta_i^2} \right) \times 100 \; i \neq 0 \qquad (6)$$

The P_i and β_i are the percentage effect and coefficient of each term. As seen, terms have both positive (+) and negative (−) effects on the AFG and COD removals. While the terms to the right of the line are significant, the terms to the left are not significant on the responses. It is clear from Fig. S3a the terms BE, BC, CD, CE, AA, DD, BB, BD, EE, AD, AE, and DE have insignificant effects on COD removal efficiency that are confirmed with the ANOVA test (p-value, see Table 6). The terms BC, EE, BB, DD, BB, DE, AA, and CD have insignificant effects on AFG removal efficiency. The results are in good agreement with ANOVA tests. The maximum percentage effects for AFG and COD removal were calculated
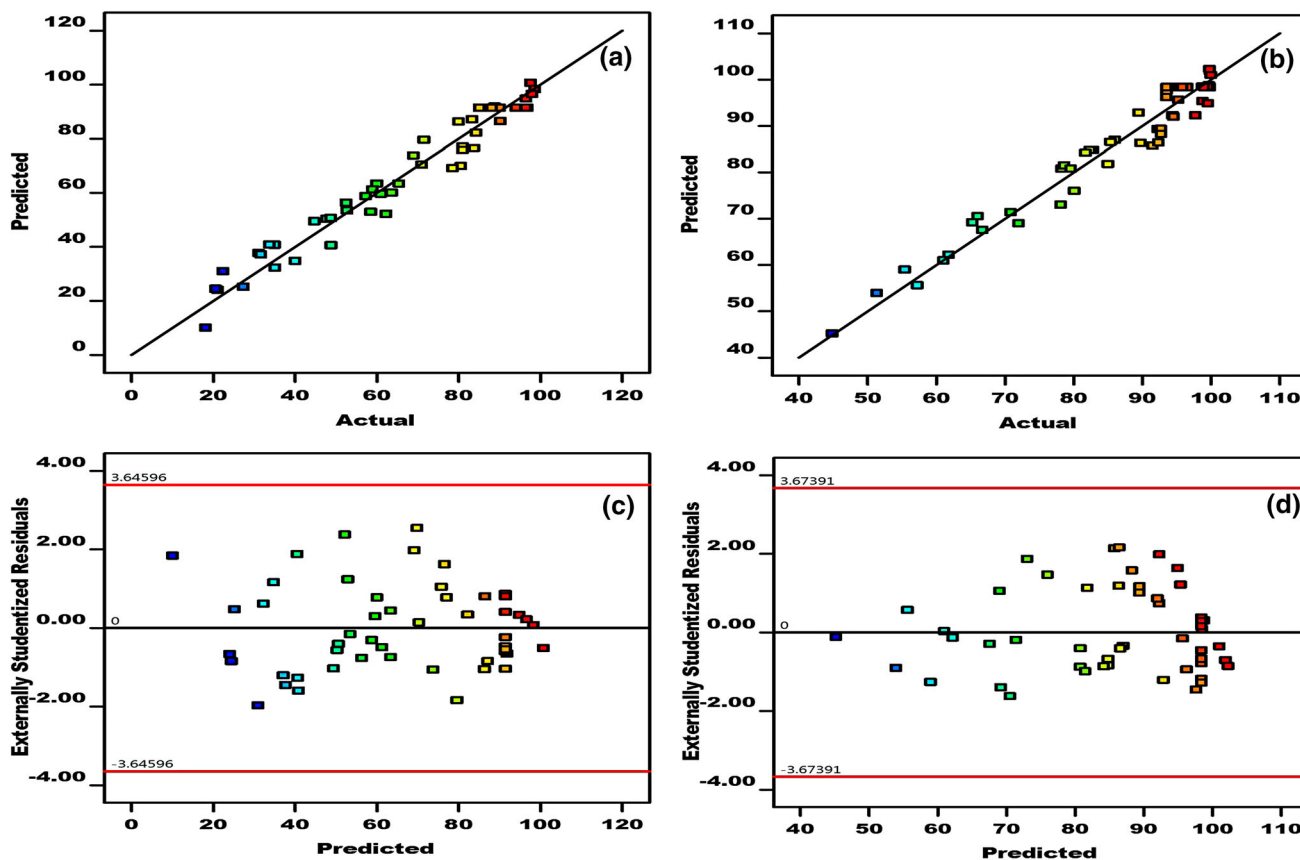
Fig. 1 Graph of predicted values vs. actual values for **a** COD removal, **b** AFG removal, predicted values vs. externally studentized residuals for **c** COD removal and **d** AFG removal

as 25.22% (for E term) and 25.88% (for B term), respectively. It is clear from Table 6 that the lack of fit values is 2.57 and 3.01 for the first and second response, respectively, which means that the lack of fit values only occurs with a probability of 10.10% and 6.93%, respectively, due to noise. The *Adequate Precision* values express the signal-to-noise ratio from the fit statistics parameter (Table 6), for COD and AFG removals are 21.502 and 22.024. It can be concluded that the signal is sufficient when a value greater than 4 is desired[18]. In the signal-to-noise ratio, the noise shows the value that should be reduced while the signal represents the value that should be maximized [50]. If the signal is more than the noise, the noise can be neglected. According to all results, the parameters individually affect both responses to a significant degree, the quadratic model established is valid, and this model can be used to navigate the design space.

Another indicator where parameter effects can be observed in parallel with the ANOVA result is 3D graphics. Figure 2 and Fig. 3 show the combined effects of system parameters on responses. Fe and H_2O_2 concentrations on COD and AFG removal can be observed in Figs. 2a and 3a, respectively. The operation conditions for the Figs. 2a and 3a are pH: 3.75, time: 37.5 min and AFG concentration:

300 mg/L, Fe^{2+} concentrations: 50–300 mg/L and of H_2O_2 concentrations: 50–600 mg/L. When Fe^{2+} conc. increased from 50 mg/L to 300 mg/L, the efficiency of COD removal increased. Also, COD removal efficiency increases when H_2O_2 conc. increases from 50 mg/L to 600 mg/L in a similar way. The removal of COD and AFG reaches almost 100% efficiency as observed in Figs. 2a and 3a.

The increased COD and AFG removal efficiency with increasing H_2O_2 concentration can be attributed to the greater production of •OH and •OOH in the wastewater (Eqs. 7 and 8).

$$Fe^{2+} + H_2O_2 \rightarrow Fe^{3+} + \bullet OH + OH^- \tag{7}$$

$$Fe^{3+} + H_2O_2 \rightarrow Fe^{2+} + \bullet OOH + H^+ \tag{8}$$
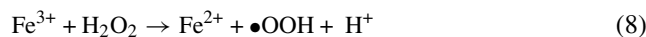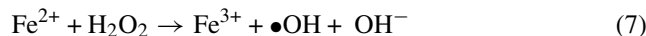
The generated radicals, shown in Eqs. 7 and 8, attack the C–H bonds of organic pollutants (symbolized by S) and initiate a series of chain reactions (Eqs. 9–13) [51]. Youssef et al. [51] stated that these chain reactions produce free radicals, and organic radicals react with dye molecules and convert them to nontoxic end products.

$$SH + \bullet OH \rightarrow \bullet S + H_2O \tag{9}$$

Table 6 Analysis of variance for response 1 and response 2

Source	Response 1 (COD Removal, %)						Response 2 (AFG Removal, %)					
	Sum of Squares	df	Mean Square	F-value	p-value		Sum of Squares	df	Mean Square	F-value	p-value	
Model	28,756.26	20	1437.81	34.28	< 0.0001	Significant	10,205.20	20	510.26	31.91	< 0.0001	Significant
A-Fe Conc	2682.47	1	2682.47	63.95	< 0.0001		789.52	1	789.52	49.37	< 0.0001	
B-H_2O_2 Conc	4299.08	1	4299.08	102.50	< 0.0001		1377.83	1	1377.83	86.16	< 0.0001	
C-pH	1392.51	1	1392.51	33.20	< 0.0001		589.64	1	589.64	36.87	< 0.0001	
D-time	893.34	1	893.34	21.30	< 0.0001		390.53	1	390.53	24.42	< 0.0001	
E-C_0 (Initial AFG Conc.)	2903.95	1	2903.95	69.23	< 0.0001		2132.22	1	2132.22	133.34	< 0.0001	
AB	822.66	1	822.66	19.61	0.0001		194.69	1	194.69	12.17	0.0016	
AC	323.53	1	323.53	7.71	0.0095		97.55	1	97.55	6.10	0.0196	
AD	5.14	1	5.14	0.1226	0.7287		270.11	1	270.11	16.89	0.0003	
AE	4.46	1	4.46	0.1064	0.7466		71.25	1	71.25	4.46	0.0435	
BC	92.79	1	92.79	2.21	0.1477		56.05	1	56.05	3.50	0.0713	
BD	12.04	1	12.04	0.2871	0.5962		76.54	1	76.54	4.79	0.0369	
BE	143.02	1	143.02	3.41	0.0750		355.18	1	355.18	22.21	< 0.0001	
CD	55.31	1	55.31	1.32	0.2602		0.0957	1	0.0957	0.0060	0.9389	
CE	50.93	1	50.93	1.21	0.2796		162.59	1	162.59	10.17	0.0034	
DE	0.4729	1	0.4729	0.0113	0.9162		5.18	1	5.18	0.3237	0.5738	
A^2	36.49	1	36.49	0.8700	0.3587		4.18	1	4.18	0.2616	0.6129	
B^2	19.13	1	19.13	0.4560	0.5048		34.42	1	34.42	2.15	0.1531	
C^2	1818.59	1	1818.59	43.36	< 0.0001		144.19	1	144.19	9.02	0.0055	
D^2	32.61	1	32.61	0.7774	0.3852		22.04	1	22.04	1.38	0.2499	
E^2	6.82	1	6.82	0.1627	0.6897		40.08	1	40.08	2.51	0.1242	
Residual	1216.36	29	41.94				463.74	29	15.99			
Lack of Fit	1082.48	22	49.20	2.57	0.1010	Not significant	419.43	22	19.06	3.01	0.0693	Not significant
Pure Error	133.88	7	19.13				44.32	7	6.33			
Cor Total	29,972.62	49					10,668.95	49				
CV (%)	9.94						4.70					
Adequate Precision	21.50											
R^2	0.9594						0.9565					

df degrees of freedom
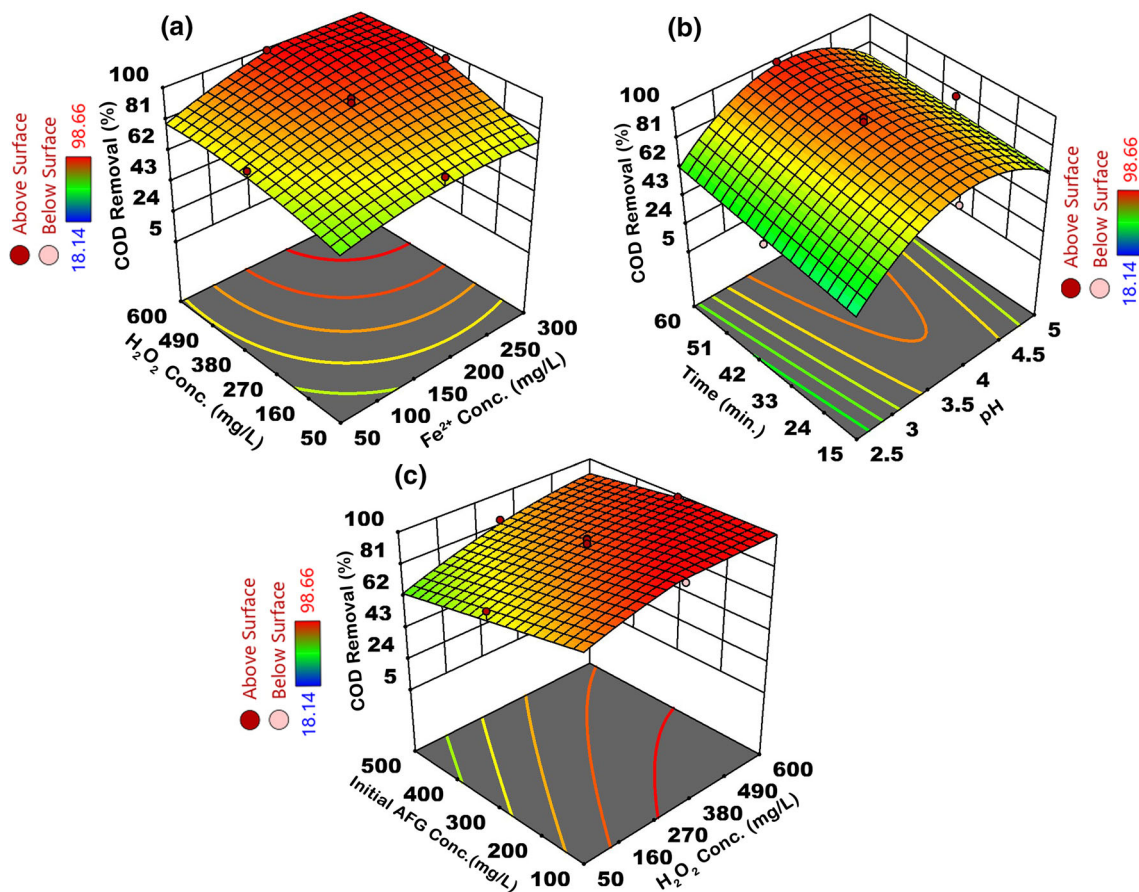
Fig. 2 Combined effect of **a** H_2O_2 Conc. and Fe^{2+} Conc. **b** Reaction time and pH **c** Initial AFG Conc. and H_2O_2 Conc. on COD removal (%)

$$SH + 2 \bullet OOH \rightarrow \bullet SOO + \bullet SO + H_2O \tag{10}$$

$$\bullet SOO + SH \rightarrow SOOH + S \tag{11}$$

$$\bullet SO + SH \rightarrow SOH + S \tag{12}$$

$$2 \bullet SOO \rightarrow SOOS + O_2 \tag{13}$$

In addition to the increase in the oxidation of organic pollutants with the increasing concentration of H_2O_2, the so-called scavenging effect can be observed when H_2O_2 is dosed at amounts greater than a critical H_2O_2 concentration (Eq. 14) [52].

$$H_2O_2 + \bullet HO \rightarrow \bullet HO_2 + H_2O \tag{14}$$
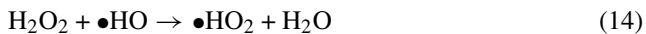
As can be seen from Eq. 14, H_2O_2 dosing above the critical concentration causes the consumption of radicals. The consumption of HO radicals, a powerful oxidizer, was reflected as a decrease in removal efficiencies. The HO_2 radical, which is formed due to the scavenging reaction of H_2O_2

with HO, has a much lower oxidizing capacity than HO radical. Additionally, the produced HO_2 radicals can react with HO radicals (Eq. 15). Consequently, these reactions cause a decrease in HO radicals.

$$\bullet HO_2 + \bullet HO \rightarrow H_2O + O_2 \tag{15}$$

All the reactions based on the scavenging of HO radicals occur because of dosing of H_2O_2 above a critical concentration. But in this study, as shown in Figs. 2a and 3a, decreasing removal efficiencies with increasing H_2O_2 concentrations were not observed. According to this observation, the critical concentration of H_2O_2 was not reached in this study.

Similarly, COD and AFG removal efficiencies increased when Fe concentration increased from 50 to 300 mg/L (Figs. 2a and 3a). Increasing Fe concentration causes H_2O_2 to decompose into more HO radicals (Eq. 7). This results in more produced HO radicals oxidizing the dye molecules (Eqs. 9–13). As seen from Eqs. 4 and 5, the Fe concentration symbolized by 'A' has a positive coefficient, indicating that the COD and AFG removal efficiencies are higher at higher Fe concentrations. In addition to individual effects, for interaction effects, there is high efficiency for both responses in
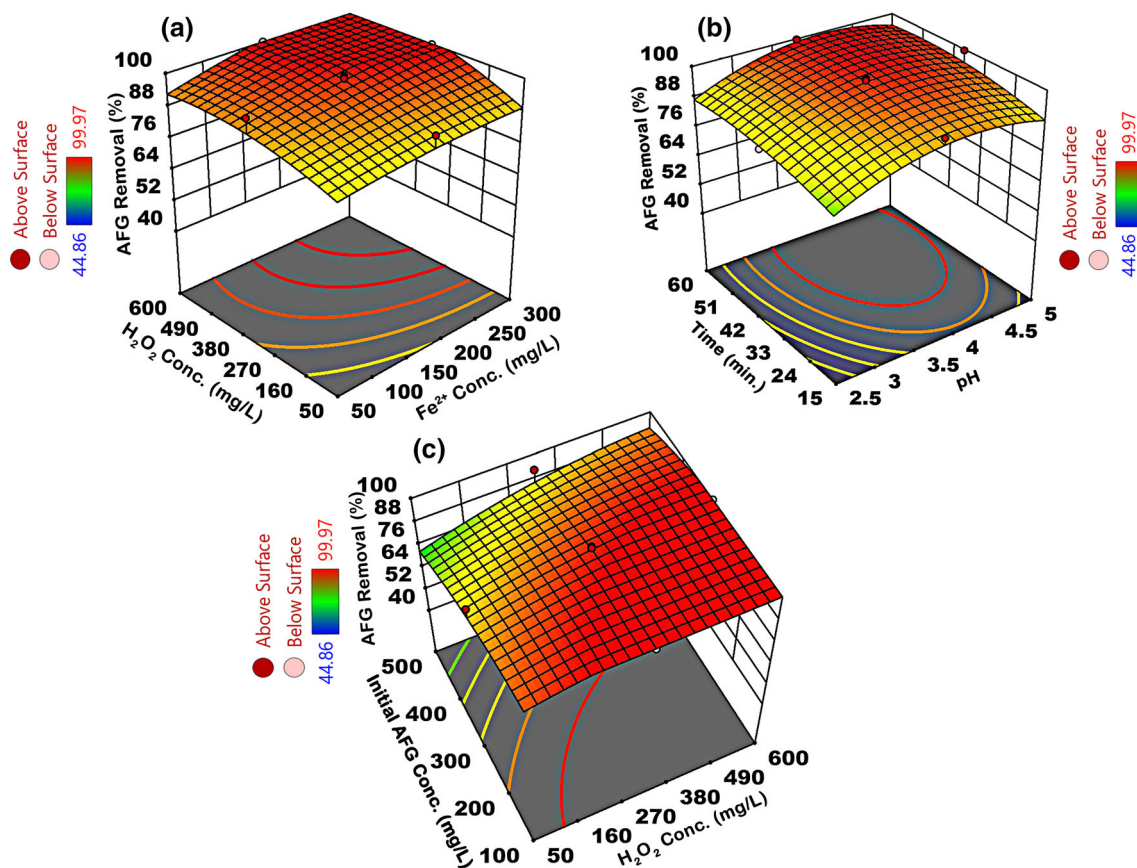
Fig. 3 Combined effect of **a** H_2O_2 Conc. and Fe.$^{2+}$ Conc. **b** Reaction time and pH **c** Initial AFG Conc. and H_2O_2 Conc. on AFG removal (%)

increasing Fe and H_2O_2 combinations. The positive 'AB' coefficient also confirms this interpretation in Eq. 4 and Eq. 5.

Figures 2b and 3b shows the combined effect of pH and time on COD and AFG removal efficiencies. The operation conditions for Figs. 2b and 3b are Fe^{2+} concentration: 175 mg/L, H_2O_2 concentration: 325 mg/L, AFG concentration: 300 mg/L, pH values: 2.5- 5, reaction times: 15–60 min. The instability of H_2O_2 in alkaline environments and the decrease in oxidizing capacity led to the investigation of the homogeneous Fenton process in more acidic conditions. For this reason, in this study, the effect of pH was investigated in the range of 2.5 to 5. When the pH value increased from 2.5 to 3.75, both removal efficiencies increased considerably. The presence of $H_2O_3^+$ at pH < 3 leads to an increase in the stability of H_2O_2; so, the generation of HO radicals is restricted [53, 54]. Equation 16 [55] shows that H^+ scavenges the HO radicals in severe acidic environments.

$$\bullet HO + H^+ + e^- \rightarrow H_2O \tag{16}$$

However, at pH above 3.75, removal efficiencies started to decrease slowly for both responses. As can be seen from Table 3, maximum removal efficiencies were observed at pH 3.75 in experiment 39. This can be explained by the rapid

decomposition of H_2O_2 by iron ions into hydroxyl radicals, leading to a rapid increase in COD and color removal efficiencies. The slightly decreased removal efficiencies at pH values above pH 3.75 can be attributed to the reduced oxidation potential of HO radicals and lower production rate of HO radicals because of hydrolysis of Fe^{3+} [52]. Similar observations were reported in the literature [52, 55, 56].

It is possible to see the effect of reaction time in Figs. 2b and 3b. The removal efficiencies for both responses increased significantly when the reaction time increased from 15 to 37.5 min. This situation can be attributed to the high amount of HO radicals in the medium in the early stages of the reaction [57]. This can result in rapid oxidation. Güneş and Cihan [58] reported in their study that with increasing reaction time, sufficient H_2O_2 can participate in the reaction to oxidize the pollutants. The low removal efficiencies observed at reaction times of less than 37.5 min may be related to insufficient HO radicals in the solution. In addition, it may be associated with the short reaction of organic substances with these radicals and the stopping of the reaction before the organic substances were sufficiently oxidized. When the reaction time increased from 37.5 to 60 min, a slow change was observed in the removal efficiencies for both responses. This situation can

be explained by the decreased amount of HO radicals in the later stages of the reaction and the corresponding decrease in the pollutant concentration [57, 59].

Figures 2c and 3c shows the combined effect of initial AFG concentration and H_2O_2 concentration. The operation conditions for Figs. 2b and 3b are Fe^{2+} concentration: 175 mg/L, pH values: 3.75, reaction time:37.5 min., H_2O_2 concentrations: 50–600 mg/L, AFG concentrations: 100–500 mg/L. The removal efficiencies for both responses decreased significantly when the initial AFG concentration increased from 100 to 500 mg/L. This decrease can be attributed to the non-parallel relationship between increasing pollutant concentration and hydroxyl radicals in the medium. In other words, the amount of organic molecules to be attacked by radicals is higher at 500 mg/L compared to 100 mg/L, and the insufficient amount of radicals in parallel can explain this situation. On the other hand, Zhang and Zhang [60] attributed a similar observation to the occurrence of side reactions, especially due to non-specific oxidation of main intermediates and competitive consumption of hydroxyl radicals, as reported by Murugananth et al. [61].

3.3 Numerical Optimization

Efficiency and economy are essential in system optimization. Optimization in RSM can be done numerically, graphically, and by the matrix method. The advantage of numeric optimization is that the experimenter can set the limits of the optimization conditions. This means limiting the parameters as desired to obtain a more economical and effective result depending on the experimental conditions, the nature of the process, and other environmental conditions. For this purpose, system input and output parameters can be set as 'target,' 'minimize,' 'maximize,' and 'in range.' The system offers many solutions that include different input–output parameters with different 'desirability' values. The experimenter should first pay attention to the 'desirability' value when choosing a solution. The closer this value is to 1.00 means that the solution is more consistent with reflecting the actual.

Maximizing the removal efficiency and minimizing the system costs as much as possible are the criteria to be considered. For this, the consumption of Fe^{2+} and H_2O_2 concentrations among system consumables was minimized to reduce system cost. Also, the pH parameter was chosen as the 'target' for the natural wastewater pH to reduce the cost. Other system parameters were targeted as 'in range.' On the other hand, COD and AFG removal efficiencies were maximized.

The system parameters were numerically optimized with these conditions: Fe^{2+}: 50 mg/L, H_2O_2: 50 mg/L, pH 3.75, R. time: 42.54 min, C_0: 100 mg/L. The desirability of these

selected conditions was 0.977. Under these conditions, the COD removal efficiency predicted by the system is 80.5%, and the AFG removal efficiency is 94.11%.

In order to verify the system optimization, an experiment was carried out under the numerically optimized conditions, and COD and AFG removal efficiencies were experimentally found to be 81.01% and 94.33%. In this case, we can say that the established model is valid, and the experimental data support the data predicted by the system.

According to the authors' best knowledge, there is no study investigating the removal of AFG (Basic Red 13) dye with the Fenton process. For this reason, the comparison of this study, which was carried out with the classical Fenton process, with other Fenton processes is given in Table 7. Fenton processes are known as advanced oxidation processes and are known as good practices in removing organic pollutants since H_2O_2 is broken down into H_2O and O_2 and converted into nontoxic products. Minimizing the use of additional chemicals (such as H_2O_2, $FeSO_4 \cdot 7H_2O$), which is among the general disadvantages of Fenton processes, also affects the applicability of the process. Another limiting factor for homogeneous Fenton processes is sludge formation, but it is possible to reuse the sludge for other applications. Fenton sludge contains densely $Fe(OH)_3$, and it has many application areas, the synthesis of magnetic heterogeneous Fenton catalysts and the recovery of Fe^{2+} from Fenton sludge, etc. (see Sect. 3.5). As seen in Table 7, Nguyen et al. [62] achieved good efficiencies for dyestuff and organic matter removal using magnetic waste iron slag composite and iron sludge as catalysts. The heterogeneous Fenton processes eliminate the use of iron (II) sulfate. Still, the industrial-scale catalyst synthesis may be more costly than using iron (II) sulfate for the homogenous Fenton process. Homogeneous Fenton processes have advantages such as applying at high organic loadings, operational simplicity, simple equipment, and facilities and providing a coagulation treatment by the co-precipitation of certain contaminants. In heterogeneous Fenton processes, it has system-limiting features such as the synthesis of the catalyst in the industrial scale as a costly procedure, the contribution degree of catalyst to oxidation, the reuse procedure, the possibility of decreasing the catalyst activity over time.

The success of Fenton processes for the removal of dyestuffs was again proven in this study. As seen from Table 7, although Fenton processes were successful for dye removal and removal of organic matter fractions such as COD or total organic carbon (TOC), homogeneous Fenton processes generally showed high performance for the removal of both pollutant fractions. Rodrigues et al. [63] optimized the process conditions, where they investigated the removal of PRH dye and TOC by the Fenton process. With the central composite design approach, they determined that the ferrous ion

Table 7 Comparison of Fenton treatments for wastewaters containing dye

Dye or Wastewater Type	Process	Iron Source	Fe^{2+} or Catalyst Conc.	H_2O_2 Conc.	Reaction Time (min)	pH	COD or TOC Removal (%)	Dye Removal (%)	References
[a]MB	Heterogeneous Fenton	Fe_2GeS_4	300 mg/L	50 mM/L	10	7	56.3	–	[64]
[b]MO							66.2	–	
[c]RhB							74.2	–	
[d]RO16	Heterogeneous Fenton	Fe_3O_4/montmorillonite	1.83 g/L	77.98 mM	60	3	85.90	–	[65]
[c]RhB	Fenton-like	Magnetic waste iron slag composite	4000 mg/L	1680 mg/L	120	3	83.33	98.48	[62]
		Iron sludge					59.75	71.84	
[b]MO	Homogenous Fenton	$FeSO_4 \cdot 7H_2O$	67 mg/L	3.53 mM	1	2	–	100	[39]
[a]MB	Homogenous Fenton	$FeSO_4 \cdot 7H_2O$	4 mM	70 mM	30	3	85	98.8	[66]
[e]SBB	Homogenous Fenton	$FeSO_4 \cdot 7H_2O$	150 mg/L	100 mg/L	30	3	–	> 80	[67]
RhB [f]AR14	Homogenous Fenton	$FeSO_4 \cdot 7H_2O$	143.88 mg/L	126.89 mg/L	30	3.71	–	RhB = 81.58 AR14 = 80.22	[68]
[g]PRH	Homogenous Fenton	$FeSO_4 \cdot 7H_2O$	0.12 mM	2.9 mM	120	3.5	52.3	99.6	[63]
[h]RM5B [i]RB5 [j]OG	Homogenous Fenton and Fenton-like	$FeSO_4 \cdot 7H_2O$	1 mg/L	200 mg/L	480	2.5–3	40	RM5B = 99 RB5 = 99 OG = 99	[52]
AFG	Homogenous Fenton	$FeSO_4 \cdot 7H_2O$	50 mg/L	50 mg/L	42.54	3.75	81.01	AFG = 94.33	**This study**
Binary dye solution (AFG + MO)							53	AFG = 68 MO = 73	
Real textile wastewater							42	[k]RY86 = 62.72 [l]AO7 = 51.73 [m]RG19 = 39.39	

[a]Methylene Blue, [b]Methyl Orange, [c]Rhodamin B, [d]Reactive Orange 16, [e]Sudan Black B, [f]Acid Red 14, [g]Procion Red H-EXL, [h]Red MX-5B, [i]Reactive Black 5, [j]Orange G, [k]Reactive Yellow 86, [l]Acid Orange 7, [m]Reactive Green 19

dosage and temperature parameters had positive and negative effects. On the other hand, they efficiently optimized the system to increase the targeted dye removal to 99.6%. As observed in this study, organic matter mineralization (TOC) was less observed in their study. This may be due to the longer reaction times required for organic matter mineralization. Hsueh et al. [52] reported (Table 7) that 99% removal was obtained for RM5B, RB5, and OG dyes removal with the Fenton process, while TOC removal was reported as only 40% with 480 min reaction time. They explained that TOC removal takes place with a slow reaction rate. In this study, homogeneous Fenton process optimization was performed only for AFG removal, and AFG removal was achieved as 94.33%. However, the Fenton process for binary dye solution and real textile wastewater under the optimized conditions for AFG and dyestuff removal was not observed to be high. This is related to which target pollutant removal is optimized according to which output parameter. Similarly, it will be possible to maximize system efficiency and to optimize system parameters when the optimization procedure is carried out for binary solution and real textile wastewater. For this reason, it would be better to use the concept of 'suitable process for the pollutant' and ' sucsessful system optimization' instead of the term 'best process.' As a result, it can be concluded that homogeneous Fenton processes are suitable for wastewater containing AFG.

3.4 Decolorization Kinetics

In this study, oxidation of organic pollutants by HO radicals was investigated by the well-known kinetic models of pseudo-first-order (PFO) and pseudo-second-order (PSO) models. Also, the BMG model was applied, as developed by Behnajady et al. [69]. The general rate law for organic molecules is displayed in Eq. 17 [66, 70];

$$r = -\frac{dC_{AFG}}{dt} = k_{HO}C_{HO}C_{AFG} + \sum_i k_{oxi}C_{oxi}C_{AFG} \quad (17)$$

oxi corresponds to oxidants except for •HO. •HOO is one of the radical species which has lower oxidation capacity than •HO. Because the concentration of •HO could be measured directly, it was assumed to be constant under some conditions. So, the concentration of •HO was considered to be a part of the apparent constant (k_{app}), which can be expressed by the PFO reaction (Eq. 18) [66, 70]. Here, $C_{t\ AFG}$ and $C_{0\ AFG}$ represent the remaining AFG concentration in the sample at t time and initial AFG concentration, respectively. k_{app1} is the apparent rate constant for PFO reaction kinetics. With a graph plotting $\ln(C_{t\ AFG}/C_{0\ AFG})$ versus t, k_{app1}

(min^{-1}) can be calculated from the slope of the line.

$$\ln \frac{C_{tAFG}}{C_{0AFG}} = -k_{app1}t \quad (18)$$

The PSO kinetic model can be summarized by Eq. 19, where k_{app1} is the apparent rate constant for the PSO reaction kinetic.

$$\frac{1}{C_{tAFG}} = \frac{1}{C_{0AFG}} + k_{app2}t \quad (19)$$

Behnajady et al. [69] derived a mathematical model to fully use the results for real applications (Eq. 20). m and b represent the characteristic constants of the BMG model. With a plot drawn of ($t/(1 - C_{t\ AFG}/C_{0\ AFG})$) versus t, b and m can be calculated from the slope and intercept of the line, respectively.

$$\frac{t}{1 - C_{tAFG}/C_{0AFG}} = m + bt \quad (20)$$

The kinetic experiments for the effect of initial AFG concentration on AFG removal rate were conducted under the conditions: Fe^{2+}: 50 mg/L, H_2O_2: 50 mg/L, and pH 3.75, which were determined as optimum. Effect of H_2O_2 concentration on AFG removal rate was explored under the conditions: Fe^{2+}: 50 mg/L, C_0: 100 mg/L, and pH 3.75. Additionally, the effect of Fe^{2+} concentration on AFG removal rate was investigated under the conditions: C_0: 100 mg/L, H_2O_2: 50 mg/L, and pH 3.75. For all kinetic studies, the samples were taken at nine different time intervals between 5 and 60 min. The regression coefficients and kinetic model constants calculated are shown in Table 8.

Figure 4 shows the effect of initial AFG, H_2O_2, and Fe^{2+} concentrations on AFG removal efficiencies with different reaction times. As shown in Fig. 4a, the same concentration of hydroxyl radicals attacks the pollutant with increasing dose reflected as a decrease in the AFG removal rate. For all concentrations of AFG, H_2O_2, and Fe^{2+} in the first 5 min, the reaction occurred rapidly and generally showed a slowing trend after 40 min (Fig. 4a–c). The degradation of dyes with homogenous Fenton processes typically depends on two steps [71]; one is the rapid degradation of dyes depending on the reaction between H_2O_2 and Fe^{2+} (Eq. 7). The second step is a reaction between H_2O_2 and Fe^{3+} (Eq. 8), where relatively slow degradation occurs. The accumulated Fe^{3+} concentrations promote the generation of •HOO, which has a low oxidation capacity on organic compounds [72]. •HOO attacks the dye molecules and degrades them to intermediate products and/or end products (Eqs. 9–13). Jafari et al. [73] reported that the decolorization of AFG (BR13), a cationic dye, occurs after breaking the azo bond and reported the intermediates they detected by GC–MS technique as a result

Table 8 Kinetic model parameters and correlation coefficients (R^2) for the decolorization of AFG

AFG Conc. (mg/L)	PFO		PSO		BMG		
	K_{app1} (min^{-1})	R^2	k_{app2} (L mg^{-1} min^{-1})	R^2	1/m (min^{-1})	1/b	R^2
25	0.032	0.9871	0.0188	0.9826	0.5506	0.9918	0.9996
50	0.028	0.9513	0.0072	0.9599	0.5952	0.9819	0.9997
100	0.027	0.9700	0.0031	0.9852	0.5499	0.9773	0.9996
200	0.021	0.9792	0.0009	0.9977	0.4666	0.9511	0.9994
300	0.015	0.9637	0.0003	0.9883	0.4035	0.8982	0.9994
400	0.011	0.9368	0.0004	0.9591	0.3376	0.8222	0.9993
500	0.008	0.9349	0.00004	0.9546	0.2467	0.7321	0.9989
H$_2$O$_2$ Conc. (mg/L)	PFO		PSO		BMG		
	K_{app1} (min^{-1})	R^2	k_{app2} (L mg^{-1} min^{-1})	R^2	1/m (min^{-1})	1/b	R^2
50	0.027	0.9700	0.0031	0.9852	0.5499	0.9773	0.9996
100	0.032	0.9961	0.0036	0.9566	0.5623	0.9925	0.9995
200	0.041	0.9395	0.0049	0.9364	0.5863	1.0092	0.9987
400	0.043	0.9888	0.0051	0.9560	0.8652	1.0095	0.9996
600	0.081	0.9668	0.0169	0.8347	1.0282	1.0152	0.9999
Fe^{2+} conc. (mg/L)	PFO		PSO		BMG		
	K_{app1} (min^{-1})	R^2	k_{app2} (L mg^{-1} min^{-1})	R^2	1/m (min^{-1})	1/b	R^2
50	0.027	0.9700	0.0031	0.9852	0.5499	0.9773	0.9996
100	0.031	0.9855	0.0033	0.9283	0.5623	0.9605	0.9989
200	0.043	0.9770	0.0047	0.9709	0.5863	0.9707	0.9994
400	0.060	0.9933	0.0058	0.9431	0.8652	1.0088	0.9996

of the oxidation of BR13 by sonoelectrochemical process (in present of TiO$_2$ nanoparticles). Figure 4b shows the increased AFG removal efficiencies with increased H$_2$O$_2$ concentrations related to more OH radicals attacking the C-H bonds of AFG molecules (Eqs. 9–13). The AFG removal was achieved slow degradation for all H$_2$O$_2$ and Fe^{2+} concentrations after 40 min which may be related to the second oxidation step of the Fenton process (Fig. 4b and c).

Beldjoudi et al. [74] reported that the degradation rate of dyes mainly depends on the HO radical concentration and H$_2$O$_2$ concentration. This situation was confirmed with the increased kinetic coefficients with increasing Fe^{2+} concentrations (Table 8). As clear from Table 8, increasing kinetic coefficients with increasing H$_2$O$_2$ concentrations indicate that the reaction rate increases. Therefore, increasing radicals increased the rate of AFG removal while the AFG concentration was constant (Fig. 4b). Most studies [75, 76] have reported an inverse relationship between increasing H$_2$O$_2$ concentrations and organic matter removal, with a series of side reactions resulting in the scavenging of radicals (Eqs. 14,15). However, this situation was not observed

in this study because the critical H$_2$O$_2$ concentration was not reached.

As seen in Table 8, With increasing AFG concentration, the apparent rate constants for PFO and PSO decrease. When the correlation coefficients between PFO and PSO are compared, PSO has relatively higher correlation coefficients. The decrease in kinetic coefficients with increasing AFG concentrations may suggest that the reaction between oxidative radicals and dye molecules and the intermediate and/or end converted products are less favoured by loaded organic pollutants. Li et al. [77] stated that the produced hydroxyl radical concentrations were the same because of constant H$_2$O$_2$ and Fe^{2+} dosages even the concentrations of dye increase. When AFG concentrations change from 50 to 500, the *1/m* and 1/b values decrease. So, this situation can be attributed to the increasing amount of AFG dye molecules that need to be oxidized. Insufficient radicals result in lower dye removal and lower degradation rate of dye molecules. Behnajady et al. [69] reported that higher *1/m* values indicate a faster initial degradation rate for dye molecules. Also, they stated that when *t* is infinite or long, *1/b* has theoretical maximum dye
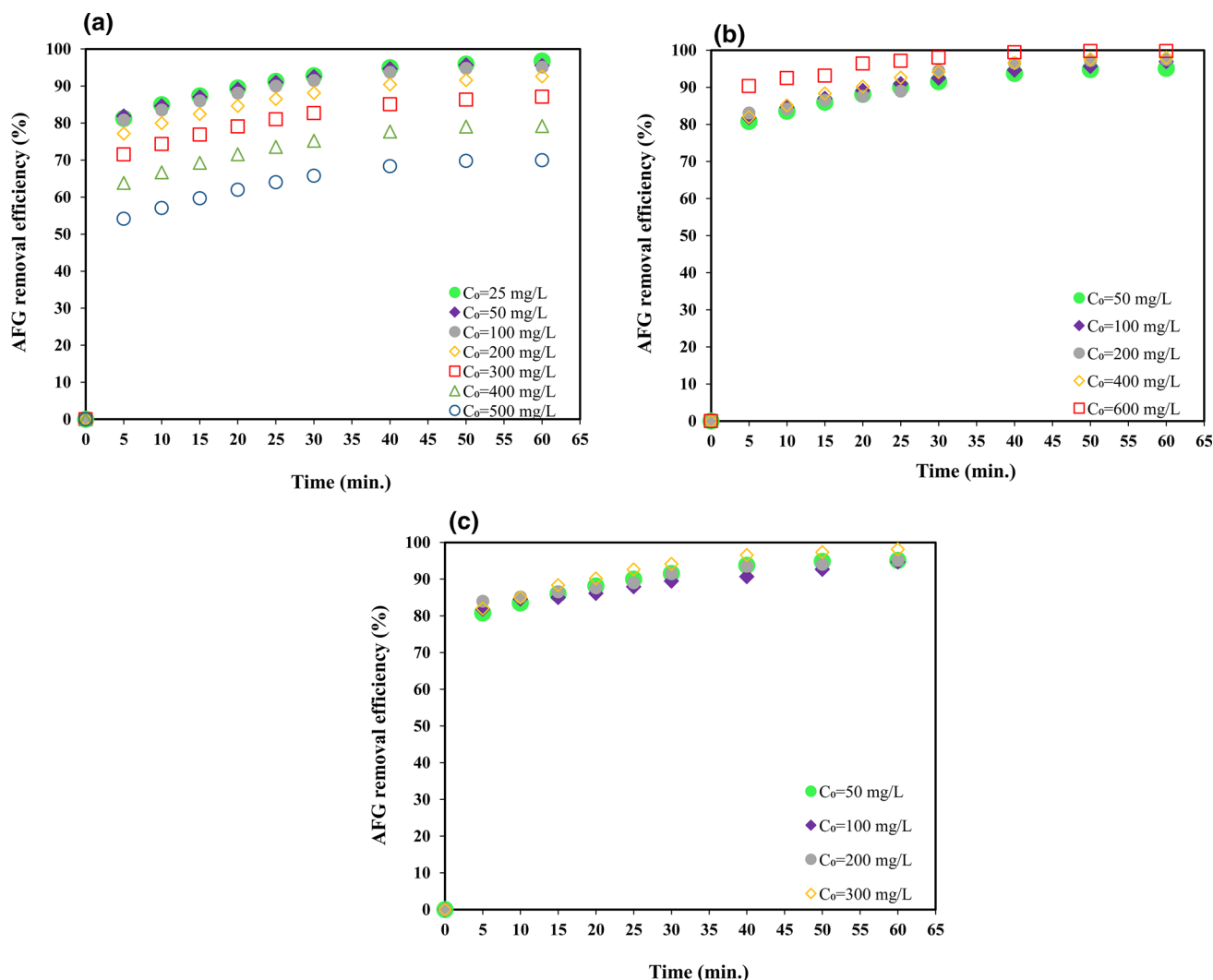
Fig. 4 The effects of **a** initial AFG, **b** H_2O_2, and **c** Fe^{2+} concentrations on AFG removal efficiencies with different reaction times

removal fraction, which means the same as the maximum oxidation capacity of the Fenton process at the end of the reaction. As seen from Table 8, $1/b$ values, in other words, maximum oxidation capacities increased with increasing H_2O_2 and Fe^{2+} concentrations. As a result of increased H_2O_2 and Fe^{2+} concentrations, the produced radical concentrations increased and accelerated the AFG degradation rate. Zhang et al. [78] stated that the $1/b$ values around 1 indicate Fenton oxidation has a potentially high oxidation capacity for pollutants. So, it can be said that the maximum oxidation capacities were achieved for 600 mg/L of H_2O_2 concentrations and 400 mg/L of Fe^{2+} concentrations.

The highest R^2 values were obtained for the BMG model for all AFG, H_2O_2, and Fe^{2+} concentrations. So, the best-fitted model for AFG degradation is the BMG model. Many studies reported the best fitting model as BMG for dye degradation with Fenton oxidation [71, 79, 80].

3.5 Fenton Sludge Generation

Sludge generation is among drawbacks of the homogenous Fenton process [81]. The Fenton process typically involves the formation of hydroxyl radicals after Fe^{2+} catalyzed reaction with H_2O_2 (Eq. 7). After the oxidation of organic substances by hydroxyl radicals, the pH value of the solution/wastewater is alkalized, and $Fe(OH)_3$ is formed in this process (Eq. 21). The $Fe(OH)_3$ flocs formed have a structure that can absorb organic and inorganic pollutants.

$$Fe^{3+} + OH^- \rightarrow Fe(OH)_3 \downarrow \tag{21}$$
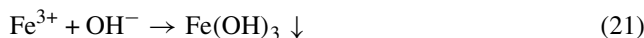
According to the results, the generated sludge under optimized conditions for AFG dye solution, binary dye solution, and real textile wastewater was 0.110 ± 0.02 g/L (6% (v/v)), 0.108 ± 0.01 g/L (5% (v/v)), and 0.120 ± 0.03 g/L (7% (v/v)), respectively. The real textile wastewater contains more

organic pollutants than dye solutions. More Fe^{2+} and H_2O_2 doses will be required for higher removal efficiencies, resulting in more sludge production. Since the doses of Fe^{2+} and H_2O_2 are constant in the solution, the formed sludge amounts are close to each other for aqueous environments.

Fenton sludge has toxic nature [82]. In a facility where the homogeneous Fenton process is applied, the first thing to do is to optimize the system to reduce sludge formation. Then, the sludge use evaluation for another application should be investigated before the sludge formed is disposed of. There are beneficial uses of Fenton sludge reported in many studies such as magnetic catalyst synthesis from ferric sludge by hydrothermal method [83], Fe^{2+} regeneration from Fenton sludge to remove pharmaceuticals from the municipal wastewater by Fenton process [84], and synthesis of catalyst using Fenton sludge as an iron source and application on the Fenton-based process for phenol removal [85].

3.6 Homogenous Fenton process performance for a binary dye solution and real textile wastewater

In order to explore the AFG removal performance of homogeneous Fenton processes in the presence of other dyes, binary solution studies were performed. For this purpose, a solution containing 50 mg/L methyl orange and AFG was treated under optimized conditions (Fe^{2+}: 50 mg/L, H_2O_2: 50 mg/L, pH 3.75, R. time: 42.54 min.). According to a previous study, the concentration of non adsorbed dyes was analyzed with UV–Vis spectroscopy [86]. After Fenton process treatment, COD removal efficiency was calculated as 53% for binary dye solution. The performance of the Fenton process based on dye and COD removal efficiencies was decreased in the presence of other dyes compared to aqueous solutions that contain only AFG dye. The AFG ($C_{22}H_{26}Cl_2N_2$) removal efficiency decreased from 94.33% to 68% in the presence of methyl orange ($C_{14}H_{14}N_3NaO_3S$) dye. However, the removal efficiency for methyl orange from the binary solution was calculated as 73%. These results highlight that the decomposition and/or degradation of pollutants depends on their chemical properties. It should be noted that binary solution purification conditions were run under AFG-optimized conditions. Therefore, these results also emphasize the importance of the optimization processes being specific to the pollutant characteristics/treatment process.

The effectiveness of the Fenton process on the removal of certain dyes from real textile industry wastewater was investigated under the optimized conditions (Fe^{2+}: 50 mg/L, H_2O_2: 50 mg/L, pH 3.75, R. time: 42.54 min.). The characteristic of wastewater is given in Table 1. The UV–Vis scan was conducted for wastewater before and after the Fenton processes. Results are shown in Fig. S4. According to the

λ (nm) values, three types of dye were estimated with the wavelengths of 410, 484, and 627 nm, which may correspond to the Reactive Yellow 86 [87], Acid Orange 7 [88], and Reactive Green 19 [89], respectively. As seen from Fig. S4, the absorbance of each dye decreased after the Fenton process, which shows the removal of dyes from wastewater. According to the results, Reactive Yellow 86 (RY86), Acid Orange 7 (AO7), and Reactive Green 19 (RG19) removals were calculated as 62.72%, 51.73%, and 39.39%, respectively. Additionally, COD removal for real textile wastewater was found as 42%.

Satisfactory yields for the removal of certain dyes from a real textile industry wastewater under AFG-optimized conditions have not been obtained because the optimized conditions for a solution containing AFG may not be suitable for aqueous media containing other dye(s) and/or wastewater. In addition, while the pollutions for AFG and binary solutions were dyes, there are complex pollutants in real wastewater. It is clear much more Fe^{2+} and H_2O_2 are required to oxidize complex pollutants, emphasizing the need for more hydroxyl radicals. It can be said that Fenton processes can be applied as pretreatment for AFG containing solutions and textile wastewaters. Considering the high removal efficiency obtained only for AFG-containing solutions in this study (94.33%), it can be said that successful results can be obtained when the optimization procedure is carried out specifically for the target pollutant and wastewater/solution type. The results emphasize that optimizing a process is very important to increase the removal efficiency even using a traditional process.

3.7 Cost Estimation

The cost estimation of the homogeneous Fenton process for the laboratory-scale treatment of wastewater containing AFG is based on chemical usage. The chemicals used are $FeSO_4 \cdot 7H_2O$, H_2O_2, $NaOH$, and HCl. Prices of chemicals were determined as a result of market research for August 2021. Total cost calculation was estimated with Eq. 22 [90].

$$\text{Total Cost} \left(\frac{\$}{m^3 \text{ treated waste water}} \right) = \$Fe^{2+} + \$H_2O_2 + \$NaOH + \$HCl \tag{22}$$

The prices were determined as 125 \$/MT, 150 \$/MT, 250 \$/MT, and 250 \$/MT for H_2O_2, $FeSO_4 \cdot 7H_2O$, $NaOH$, and HCl respectively. To achieve 94.33% dye removal and 81.01% COD removal, the total experimental cost to treat one m^3 AFG solution was calculated as \$ 0.26 at the laboratory scale. It should be noted that these cost calculations are for conditions optimized for a single AFG solution with a low

COD load. Asghar et al. [91] optimized with Taguchi coupled with principal component analysis (PCA) to treat textile industry wastewater with the homogeneous Fenton process. They reported that the experimental cost was reduced by $54/m^3. Pliego et al. [92] reported that these costs depend on the capacity of the wastewater plant, the nature and concentration of pollutants, and reactor properties for a full-scale system. Industrial wastewaters have high organic loads (COD, TOC), and it may be possible to treat this wastewater on an industrial scale with much higher costs. In this case, it will be possible to optimize the operating parameters according to the high-efficiency low-cost principle. This study demonstrated that one of the best practices for cost and system optimization is RSM.

4 Conclusion

The homogeneous Fenton process was investigated and optimized with a central composite design to remove AFG and COD. The established quadratic model was reliable and sufficient to predict the experimental data. The operating parameters significantly affected AFG and COD removal individually. Optimum conditions were determined as Fe^{2+}: 50 mg/L, H_2O_2: 50 mg/L, pH 3.75, R. time: 42.54 min, C_0: 100 mg/L. Under these conditions, COD and AFG removals were determined experimentally as 81.01% and 94.33% and confirmed theoretically. According to the kinetic results, the rapid oxidation for AFG removal occurred in 5 min and slow oxidation was observed after 40 min. The performance of the Fenton treatment was evaluated for binary solutions containing Methyl Orange and AFG and for real textile wastewater containing Reactive Yellow 86, Acid Orange 7, and Reactive Green 19 dyes. The generated sludge for AFG dye solution, binary dye solution, and real textile wastewater was 0.110 ± 0.02 g/L (6% (v/v)), 0.108 ± 0.01 g/L (5% (v/v)), and 0.120 ± 0.03 g/L (7% (v/v)), respectively. The experimental cost estimation based on chemical consumption was calculated as $0.26 for 1 m^3 of AFG solution treatment. In this study, the high removal efficiencies of AFG-containing solutions in which numerical optimization is applied, and low removal efficiencies observed in binary and real wastewater where numerical optimization is not applied highlight the importance of the optimization procedure. High removal efficiencies can be achieved by providing the optimization procedure for solutions or wastewaters containing various dyes.

Author Contributions DO contributed to conceptualization, investigation, experimentation, methodology, software using, data analysis, supervision, validation, visualization, writing–original draft, writing–review and editing, and AO contributed to investigation, experimentation, methodology, data analysis, validation, writing–original draft, writing–review and editing.

References

1. Easton, J. R., Waters, B. D., Churchley, J. H., Harrison, J.: Colour in dyehouse effluent. Society of Dyers and Colourists (1995)
2. Elkady, M.F.; Ibrahim, A.M.; El-Latif, M.M.A.: Assessment of the adsorption kinetics, equilibrium and thermodynamic for the potential removal of reactive red dye using eggshell biocomposite beads. Desalination (2011). https://doi.org/10.1016/j.desal.2011.05.063
3. Ozturk, D.; Sahan, T.; Bayram, T.; Erkus, A.: Application of response surface methodology (RSM) to optimize the adsorption conditions of cationic basic yellow 2 onto pumice samples as a new adsorbent. Fresenius Environ. Bull. **26**, 3285–3292 (2017)
4. Khan, I.; Luo, M.; Guo, L.; Khan, S.; Shah, S.A.; Khan, I.; Khan, A.; Wang, C.; Ai, B.; Zaman, S.: Synthesis of phosphate-bridged g-C3N4/LaFeO3 nanosheets Z-scheme nanocomposites as efficient visible photocatalysts for CO2 reduction and malachite green degradation. Appl. Catal. A Gen. **629**, 118418 (2022). https://doi.org/10.1016/j.apcata.2021.118418
5. Yönten, V.; Sanyürek, N.K.; Kivanç, M.R.: A thermodynamic and kinetic approach to adsorption of methyl orange from aqueous solution using a low cost activated carbon prepared from *Vitis vinifera* L. Surf. Interfaces. **20**, 100529 (2020). https://doi.org/10.1016/j.surfin.2020.100529
6. Castro, F.D.; Bassin, J.P.; Alves, T.L.M.; Sant'Anna, G.L.; Dezotti, M.: Reactive Orange 16 dye degradation in anaerobic and aerobic MBBR coupled with ozonation: addressing pathways and performance. Int. J. Environ. Sci. Technol. **18**, 1991–2010 (2021). https://doi.org/10.1007/s13762-020-02983-8
7. Krishnan, J.; Arvind Kishore, A.; Suresh, A.; Madhumeetha, B.; Gnana Prakash, D.: Effect of pH, inoculum dose and initial dye concentration on the removal of azo dye mixture under aerobic conditions. Int. Biodeterior. Biodegrad. **119**, 16–27 (2017). https://doi.org/10.1016/j.ibiod.2016.11.024
8. Daneshvar, N.; Oladegaragoze, A.; Djafarzadeh, N.: Decolorization of basic dye solutions by electrocoagulation: an investigation of the effect of operational parameters. J. Hazard. Mater. (2006). https://doi.org/10.1016/j.jhazmat.2005.08.033
9. Nery, V. Del; Nardi, I. De; Resources, M.D.-; conservation, undefined; 2007, undefined: Long-term operating performance of a poultry slaughterhouse wastewater treatment plant. Elsevier.
10. Liu, L.; Chen, Z.; Zhang, J.; Shan, D.; Wu, Y.; Bai, L.; Wang, B.: Treatment of industrial dye wastewater and pharmaceutical residue wastewater by advanced oxidation processes and its combination with nanocatalysts: A review. J. Water Process Eng. **42**, 102122 (2021). https://doi.org/10.1016/j.jwpe.2021.102122
11. Hussain, S.M.; Hussain, T.; Faryad, M.; Ali, Q.; Ali, S.; Rizwan, M.; Hussain, A.I.; Ray, M.B.; Chatha, S.A.S.: Emerging aspects of photo-catalysts (TiO2 & ZnO) doped zeolites and advanced oxidation processes for degradation of azo dyes: a review Curr. Anal. Chem. **17**(82), 97 (2020). https://doi.org/10.2174/1573411016999200711143225
12. Ozturk, D.; Yilmaz, A.E.: Investigation of electrochemical degradation of Basic Red 13 dye in aqueous solutions based on COD removal: numerical optimization approach. Int. J. Environ. Sci. Technol. **17**, 3099–3110 (2020). https://doi.org/10.1007/s13762-020-02692-2

13. Quanfang, L.; Jie, Y.; Cailing, Y.; Minrui, L.: Degradation mechanism of Astrazon Pink FG solution by glow discharge electrolysis. CIESC J. **69**, 2664–2671 (2018). https://doi.org/10.11949/j.issn.0438-1157.20171310

14. Sen Gupta, S.K.: Contact glow discharge electrolysis: its origin, plasma diagnostics and non-faradaic chemical effects. Plasma Sources Sci. Technol. **24**, 063001 (2015). https://doi.org/10.1088/0963-0252/24/6/063001

15. Hasija, V.; Nguyen, V.H.; Kumar, A.; Raizada, P.; Krishnan, V.; Khan, A.A.P.; Singh, P.; Lichtfouse, E.; Wang, C.; Huong, P.T.: Advanced activation of persulfate by polymeric g-C3N4 based photocatalysts for environmental remediation: a review. J. Hazard. Mater. **413**, 125324 (2021). https://doi.org/10.1016/j.jhazmat.2021.125324

16. Bhat, A.P.; Gogate, P.R.: Degradation of nitrogen-containing hazardous compounds using advanced oxidation processes: A review on aliphatic and aromatic amines, dyes, and pesticides. J. Hazard. Mater. **403**, 123657 (2021). https://doi.org/10.1016/j.jhazmat.2020.123657

17. De León, M.A.; Sergio, M.; Bussi, J.: Iron-pillared clays as catalysts for dye removal by the heterogeneous photo-Fenton technique. React. Kinet. Mech. Catal. **110**, 101–117 (2013). https://doi.org/10.1007/s11144-013-0593-y

18. Ozturk, D.: Fe3O4/Mn3O4/ZnO-rGO hybrid quaternary nanocatalyst for effective treatment of tannery wastewater with the heterogeneous electro-Fenton process: process optimization. Sci. Total Environ. **828**, 154473 (2022). https://doi.org/10.1016/j.scitotenv.2022.154473

19. Sudhaik, A.; Parwaz Khan, A.A.; Raizada, P.; Nguyen, V.-H.; Van Le, Q.; Asiri, A.M.; Singh, P.: Strategies based review on near-infrared light-driven bismuth nanocomposites for environmental pollutants degradation. Chemosphere. **291**, 132781 (2021). https://doi.org/10.1016/j.chemosphere.2021.132781

20. Manea, Y.K.; Khan, A.M.; Wani, A.A.; Saleh, M.A.S.; Qashqoosh, M.T.A.; Shahadat, M.; Rezakazemi, M.: In-grown flower like Al-Li/Th-LDH@CNT nanocomposite for enhanced photocatalytic degradation of MG dye and selective adsorption of Cr (VI). J. Environ. Chem. Eng. **10**, 106848 (2022). https://doi.org/10.1016/j.jece.2021.106848

21. Bhaumik, M.; Maity, A.; Brink, H.G.: Metallic nickel nanoparticles supported polyaniline nanotubes as heterogeneous Fenton-like catalyst for the degradation of brilliant green dye in aqueous solution. J. Colloid Interface Sci. **611**, 408–420 (2022). https://doi.org/10.1016/j.jcis.2021.11.181

22. Mahmud, N.; Benamor, A.; Nasser, M.S.; Ba-Abbad, M.M.; El-Naas, M.H.; Mohammad, A.W.: Effective heterogeneous fenton-like degradation of malachite green dye using the core-shell Fe$_3$O$_4$ @S$_i$O$_2$ nano-catalyst. ChemistrySelect **6**, 865–875 (2021). https://doi.org/10.1002/slct.202003937

23. Modarresi-Motlagh, S.; Bahadori, F.; Ghadiri, M.; Afghan, A.: Enhancing Fenton-like oxidation of crystal violet over Fe/ZSM-5 in a plug flow reactor. React. Kinet. Mech. Catal. **133**, 1061–1073 (2021). https://doi.org/10.1007/s11144-021-02001-z

24. Tabaï, A.; Bechiri, O.; Abbessi, M.: Degradation of organic dye using a new homogeneous Fenton-like system based on hydrogen peroxide and a recyclable Dawson-type heteropolyanion. Int. J. Ind. Chem. **8**, 83–89 (2017). https://doi.org/10.1007/s40090-016-0104-x

25. Modak, J.B.; Bhowal, A.; Datta, S.; Karmakar, S.: Continuous decolorization of dye solution by homogeneous Fenton process in a rotating packed bed reactor. Int. J. Environ. Sci. Technol. **17**, 1691–1702 (2020). https://doi.org/10.1007/s13762-019-02548-4

26. Lalwani, J.; Thatikonda, S.; Challapalli, S.: Varying efficacies of Fenton's oxidation treatment on pharmaceutical industry effluents of contrasting viscosity profiles. CLEAN Soil, Air, Water **49**(3), 2000335 (2021). https://doi.org/10.1002/clen.202000335

27. Şahan, T.; Öztürk, D.: Investigation of Pb(II) adsorption onto pumice samples: application of optimization method based on fractional factorial design and response surface methodology. Clean Technol. Environ. Policy. **16**, 819–831 (2014). https://doi.org/10.1007/s10098-013-0673-8

28. Mandal, T.; Maity, S.; Dasgupta, D.; Datta, S.: Advanced oxidation process and biotreatment: their roles in combined industrial wastewater treatment. Desalination **250**, 87–94 (2010). https://doi.org/10.1016/j.desal.2009.04.012

29. Eaton, A.: Measuring UV-absorbing organics: a standard method. J. Am. Water Works Assoc. (1995). https://doi.org/10.1002/j.1551-8833.1995.tb06320.x

30. Ekmekyapar Torun, F.; Cengiz, İ.; Kul, S.: Investigation of olive mill wastewater treatment with advanced oxidation processes. J. Inst. Sci. Technol. 1597–1606 (2020). https://doi.org/10.21597/jist.687345

31. Talinli, I.; Anderson, G.K.: Interference of hydrogen peroxide on the standard cod test. Water Res. **26**, 107–110 (1992). https://doi.org/10.1016/0043-1354(92)90118-N

32. Benatti, C.T.; Tavares, C.R.G.; Guedes, T.A.: Optimization of Fenton's oxidation of chemical laboratory wastewaters using the response surface methodology. J. Environ. Manage. **80**, 66–74 (2006). https://doi.org/10.1016/j.jenvman.2005.08.014

33. Hatami, M.; Domairry, G.; Mirzababaei, S.N.: Experimental investigation of preparing and using the H 2 O based nanofluids in the heating process of HVAC system model. Int. J. Hydrogen Energy. **42**, 7820–7825 (2017). https://doi.org/10.1016/j.ijhydene.2016.12.104

34. Ighalo, J.O.; Adeniyi, A.G.; Eletta, O.A.A.; Ojetimi, N.I.; Ajala, O.J.: Evaluation of Luffa cylindrica fibres in a biomass packed bed for the treatment of fish pond effluent before environmental release. Sustain. Water Resour. Manag. **6**, 120 (2020). https://doi.org/10.1007/s40899-020-00485-6

35. Aniyikaiye, T.; Oluseyi, T.; Odiyo, J.; Edokpayi, J.: Physico-chemical analysis of wastewater discharge from selected paint industries in Lagos, Nigeria. Int. J. Environ. Res. Public Health. **16**, 1235 (2019). https://doi.org/10.3390/ijerph16071235

36. APHA Awwa WEF: Standard methods for the examination of water and wastewater. American Public Health Association, Washington DC (2012)

37. Punzi, M.; Mattiasson, B.; Jonstrup, M.: Treatment of synthetic textile wastewater by homogeneous and heterogeneous photo-Fenton oxidation. J. Photochem. Photobiol. A Chem. **248**, 30–35 (2012). https://doi.org/10.1016/j.jphotochem.2012.07.017

38. Dada, M.; Popoola, P.; Mathe, N.; Pityana, S.; Adeosun, S.: Parametric optimization of laser deposited high entropy alloys using response surface methodology (RSM). Int. J. Adv. Manuf. Technol. **109**, 2719–2732 (2020). https://doi.org/10.1007/s00170-020-05781-1

39. Beldjoudi, S.; Kouachi, K.; Bourouina-Bacha, S.; Bouchene, H.; Deflaoui, O.; Lafaye, G.: Experimental and theoretical investigation of a homogeneous Fenton process for the degradation of an azo dye in batch reactor. React. Kinet. Mech. Catal. **133**, 139–155 (2021). https://doi.org/10.1007/s11144-021-01979-w

40. Öztürk, D.; Şahan, T.: Design and optimization of Cu(II) adsorption conditions from aqueous solutions by low-cost adsorbent pumice with response surface methodology. Polish J. Environ. Stud. **24**, 1749–1756 (2015). https://doi.org/10.15244/pjoes/40270

41. Ozturk, D.; Dagdas, E.; Fil, B.; Bashir, M.J.K.: Central composite modeling for electrochemical degradation of paint manufacturing plant wastewater: one-step/two-response optimization. Environ. Technol. Innov. **21**, 101264 (2020). https://doi.org/10.1016/j.eti.2020.101264

42. Kıvanç, M.R.; Yönten, V.: A statistical optimization of methylene blue removal from aqueous solutions by Agaricus Campestris using

multi-step experimental design with response surface methodology: Isotherm, kinetic and thermodynamic studies. Surf. Interfaces. **18**, 100414 (2020). https://doi.org/10.1016/j.surfin.2019.100414

43. Karimi, B.; Rokhzadi, A.; Rahimi, A.R.: RSM modeling of nitrogen use efficiency, biomass and essential oil of *Salvia officinalis* L. as affected by fertilization and plant density. J. Plant Nutr. **44**, 1067–1084 (2021). https://doi.org/10.1080/01904167.2021.1871756

44. Islam, A.; Chauhan, A.; Javed, H.; Rais, S.; Ahmad, I.: Magnetic carbon nanotubes-silica binary composite for effective Pb (II) sequestration from industrial effluents: multivariate process optimization. CLEAN Soil, Air, Water **49**(8), 2000401 (2021). https://doi.org/10.1002/clen.202000401

45. Sridhar, R.; Sivakumar, V.; Thirugnanasambandham, K.: Response surface modeling and optimization of upflow anaerobic sludge blanket reactor process parameters for the treatment of bagasse based pulp and paper industry wastewater. Desalin. Water Treat. 1–12 (2015). https://doi.org/10.1080/19443994.2014.999712

46. Radhwan, H.; Shayfull, Z.; Farizuan, M.R.; Effendi, M.S.M.; Irfan, A.R.: Optimization parameter effects on the quality surface finish of the three-dimensional printing (3D-printing) fused deposition modeling (FDM) using RSM. Presented at the (2019)

47. Bhattacharya, S.S.; Banerjee, R.: Laccase mediated biodegradation of 2,4-dichlorophenol using response surface methodology. Chemosphere (2008). https://doi.org/10.1016/j.chemosphere.2008.05.005

48. Barahimi, V.; Mehrabani-Zeinabad, A.; Rahmati, M.; Ghafaripoor, M.: Synthesis, characterization, and evaluations of Cu-doped TiO2/Bi2O3 nanocomposite for Direct red 16 azo dye decolorization under visible light irradiation. Desalin. WATER Treat. **202**, 450–461 (2020). https://doi.org/10.5004/dwt.2020.26165

49. Manmai, N.; Unpaprom, Y.; Ramaraj, R.: Bioethanol production from sunflower stalk: application of chemical and biological pretreatments by response surface methodology (RSM). Biomass Convers. Biorefinery. **11**, 1759–1773 (2021). https://doi.org/10.1007/s13399-020-00602-7

50. Prasath, K.M.; Pradheep, T.; Suresh, S.: Application of Taguchi and response surface methodology (RSM) in steel turning process to improve surface roughness and material removal rate. Mater. Today Proc. **5**, 24622–24631 (2018). https://doi.org/10.1016/j.matpr.2018.10.260

51. Youssef, N.A.; Shaban, S.A.; Ibrahim, F.A.; Mahmoud, A.S.: Degradation of methyl orange using Fenton catalytic reaction. Egypt. J. Pet. **25**, 317–321 (2016). https://doi.org/10.1016/j.ejpe.2015.07.017

52. Hsueh, C.L.; Huang, Y.H.; Wang, C.C.; Chen, C.Y.: Degradation of azo dyes using low iron concentration of Fenton and Fenton-like system. Chemosphere **58**, 1409–1414 (2005). https://doi.org/10.1016/j.chemosphere.2004.09.091

53. Sun, S.-P.; Li, C.-J.; Sun, J.-H.; Shi, S.-H.; Fan, M.-H.; Zhou, Q.: Decolorization of an azo dye Orange G in aqueous solution by Fenton oxidation process: Effect of system parameters and kinetic study. J. Hazard. Mater. **161**, 1052–1057 (2009). https://doi.org/10.1016/j.jhazmat.2008.04.080

54. Kwon, B.G.; Lee, D.S.; Kang, N.; Yoon, J.: Characteristics of p-chlorophenol oxidation by Fenton's reagent. Water Res. **33**, 2110–2118 (1999). https://doi.org/10.1016/S0043-1354(98)00428-X

55. Toprak, D.; Sener, S. (2021) Sentetik tekstil atıksuyunun fenton ve ultrases-fenton oksidasyon yöntemleri ile renk ve Koi gideriminin araştırılması. Ömer Halisdemir Üniversitesi Mühendislik Bilim. Derg https://doi.org/10.28948/ngumuh.749438

56. Bayhan, Y.K.; Değermenci, G.D.: Kozmetik atık sularından fenton prosesiyle organik madde gideriminin ve kinetiğinin incelenmesi. Gazi Üniversitesi Mühendislik-Mimarlık Fakültesi Derg https://doi.org/10.17341/gazimmfd.300609

57. Mirzaei, A.; Chen, Z.; Haghighat, F.; Yerushalmi, L.: Removal of pharmaceuticals from water by homo/heterogonous Fenton-type processes—a review. Chemosphere **174**, 665–688 (2017). https://doi.org/10.1016/j.chemosphere.2017.02.019

58. Güneş, E.; Cihan, M.T.: COD and color removal from wastewaters: optimization of Fenton process. Pamukkale Univ. J. Eng. Sci. **21**, 239–247 (2015). https://doi.org/10.5505/pajes.2014.37928

59. Alalm, M.G.; Tawfik, A.; Ookawara, S.: Degradation of four pharmaceuticals by solar photo-Fenton process: kinetics and costs estimation. J. Environ. Chem. Eng. **3**, 46–51 (2015). https://doi.org/10.1016/j.jece.2014.12.009

60. Zhang, H.; Fu, H.; Zhang, D.: Degradation of C.I. Acid Orange 7 by ultrasound enhanced heterogeneous Fenton-like process. J. Hazard. Mater. **172**, 654–660 (2009). https://doi.org/10.1016/j.jhazmat.2009.07.047

61. Muruganandhan, M.; Yoshihara, S.; Rakuma, T.; Shirakashi, T.: Mineralization of bisphenol A (BPA) by anodic oxidation with boron-doped diamond (BDD) electrode. J. Hazard. Mater. **154**, 213–220 (2008). https://doi.org/10.1016/j.jhazmat.2007.10.011

62. Nguyen, L.H.; Van, H.T.; Ngo, Q.N.; Thai, V.N.; Hoang, V.H.; Hai, N.T.T.: Improving Fenton-like oxidation of Rhodamin B using a new catalyst based on magnetic/iron-containing waste slag composite. Environ. Technol. Innov. **23**, 101582 (2021). https://doi.org/10.1016/j.eti.2021.101582

63. Rodrigues, C.S.D.; Madeira, L.M.; Boaventura, R.A.R.: Optimization of the azo dye Procion Red H-EXL degradation by Fenton's reagent using experimental design. J. Hazard. Mater. **164**, 987–994 (2009). https://doi.org/10.1016/J.JHAZMAT.2008.08.109

64. Shi, X.; Tian, A.; You, J.; Yang, H.; Wang, Y.; Xue, X.: Degradation of organic dyes by a new heterogeneous Fenton reagent - Fe2GeS4 nanoparticle. J. Hazard. Mater. **353**, 182–189 (2018). https://doi.org/10.1016/j.jhazmat.2018.04.018

65. Öztürk, D.: Degradation of Reactive Orange 16 dye with heterogeneous Fenton Process using magnetic nano-sized clay as catalyst: a central composite optimization study. Hacettepe J. Biol. Chem. **50**, 113–129 (2021). https://doi.org/10.15671/hjbc.937728

66. Giwa, A.-R.A.; Bello, I.A.; Olabintan, A.B.; Bello, O.S.; Saleh, T.A.: Kinetic and thermodynamic studies of fenton oxidative decolorization of methylene blue. Heliyon. **6**, e04454 (2020). https://doi.org/10.1016/j.heliyon.2020.e04454

67. Suhan, M.B.K.; Mahtab, S.M.T.; Aziz, W.; Akter, S.; Islam, M.S.: Sudan black B dye degradation in aqueous solution by Fenton oxidation process: kinetics and cost analysis. Case Stud. Chem. Environ. Eng. **4**, 100126 (2021). https://doi.org/10.1016/J.CSCEE.2021.100126

68. Alıasgharlou, N.; Bahram, M.; Zolfagharı, P.; Mohsenı, N.: Modeling and optimization of simultaneous degradation of rhodamine B and acid red 14 binary solution by homogeneous Fenton reaction: a chemometrics approach. Turkish J. Chem. **44**, 987–1001 (2020). https://doi.org/10.3906/kim-2002-59

69. Behnajady, M.A.; Modirshahla, N.; Ghanbary, F.: A kinetic model for the decolorization of C.I. Acid Yellow 23 by Fenton process. J. Hazard. Mater. **148**, 98–102 (2007). https://doi.org/10.1016/j.jhazmat.2007.02.003

70. Hashemian, S.: Fenton-like oxidation of malachite green solutions: kinetic and thermodynamic study. J. Chem. **2013**, 1–7 (2013). https://doi.org/10.1155/2013/809318

71. Sidney Santana, C.; Nicodemos Ramos, M.D.; Vieira Velloso, C.C.; Aguiar, A.: Kinetic Evaluation of dye decolorization by fenton processes in the presence of 3-hydroxyanthranilic acid. Int. J. Environ. Res. Public Health. **16**, 1602 (2019). https://doi.org/10.3390/ijerph16091602

72. Lima, J.P.P.; Tabelini, C.H.B.; Ramos, M.D.N.; Aguiar, A.: Kinetic evaluation of bismarck brown y azo dye oxidation by Fenton processes in the presence of aromatic mediators. Water, Air, Soil Pollut. **232**, 321 (2021). https://doi.org/10.1007/s11270-021-05258-1

73. Jafari, S.; Dehghani, M.; Nasirizadeh, N.; Akrami, H.R.: Voltammetric determination of Basic Red 13 during its sonoelectrocatalytic degradation. Microchim. Acta. **184**, 4459–4468 (2017). https://doi.org/10.1007/s00604-017-2482-y

74. Beldjoudi, S.; Kouachi, K.; Bourouina-Bacha, S.; Lafaye, G.; Soualah, A.: Kinetic study of methyl orange decolorization by the Fenton process based on fractional factorial design. React. Kinet. Mech. Catal. **130**, 1123–1140 (2020). https://doi.org/10.1007/s11144-020-01803-x

75. da Santana, R.M.; Napoleão, D.C.; Duarte, M.M.M.B.: Treatment of textile matrices using Fenton processes influence of operational parameters on degradation kinetics, ecotoxicity evaluation and application in real wastewater. J. Environ. Sci. Heal. Part A. **56**, 1165–1178 (2021). https://doi.org/10.1080/10934529.2021.1965816

76. Babuponnusami, A.; Muthukumar, K.: Degradation of phenol in aqueous solution by Fenton, Sono-fenton and Sono-photo-fenton methods. CLEAN Soil, Air, Water. **39**, 142–147 (2011). https://doi.org/10.1002/clen.201000072

77. Li, H.; Li, Y.; Xiang, L.; Huang, Q.; Qiu, J.; Zhang, H.; Sivaiah, M.V.; Baron, F.; Barrault, J.; Petit, S.; Valange, S.: Heterogeneous photo-Fenton decolorization of Orange II over Al-pillared Fe-smectite: response surface approach, degradation pathway, and toxicity evaluation. J. Hazard. Mater. **287**, 32–41 (2015). https://doi.org/10.1016/j.jhazmat.2015.01.023

78. Zhang, Q.; Wang, C.; Lei, Y.: Fenton's oxidation kinetics, pathway, and toxicity evaluation of diethyl phthalate in aqueous solution. J. Adv. Oxid. Technol. (2016). https://doi.org/10.1515/jaots-2016-0117

79. Ertugay, N.; Acar, F.N.: Removal of COD and color from Direct Blue 71 azo dye wastewater by Fenton's oxidation: Kinetic study. Arab. J. Chem. **10**, S1158–S1163 (2017). https://doi.org/10.1016/j.arabjc.2013.02.009

80. Khan, N.-U.-H.; Bhatti, H.N.; Iqbal, M.; Nazir, A.: Decolorization of Basic Turquise Blue X-GB and Basic Blue X-GRRL by the Fenton's Process and its Kinetics. Zeitschrift für Phys. Chemie. **233**, 361–373 (2019). https://doi.org/10.1515/zpch-2018-1194

81. Tong, S.; Shen, J.; Jiang, X.; Li, J.; Sun, X.; Xu, Z.; Chen, D.: Recycle of Fenton sludge through one-step synthesis of aminated magnetic hydrochar for Pb2+ removal from wastewater. J. Hazard. Mater. **406**, 124581 (2021). https://doi.org/10.1016/j.jhazmat.2020.124581

82. Gao, L.; Cao, Y.; Wang, L.; Li, S.: A review on sustainable reuse applications of Fenton sludge during wastewater treatment. Front. Environ. Sci. Eng. **16**, 77 (2022). https://doi.org/10.1007/s11783-021-1511-6

83. Zhang, H.; Xue, G.; Chen, H.; Li, X.: Hydrothermal synthesizing sludge-based magnetite catalyst from ferric sludge and biosolids: Formation mechanism and catalytic performance. Sci. Total Environ. **697**, 133986 (2019). https://doi.org/10.1016/J.SCITOTENV.2019.133986

84. Wang, G.; Tang, K.; Jiang, Y.; Andersen, H.R.; Zhang, Y.: Regeneration of Fe(II) from Fenton-derived ferric sludge using a novel biocathode. Bioresour. Technol. **318**, 124195 (2020). https://doi.org/10.1016/J.BIORTECH.2020.124195

85. Zhang, H.; Liu, J.; Ou, C.; Shen, J.; Yu, H.; Jiao, Z.; Han, W.; Sun, X.; Li, J.; Wang, L.: Reuse of Fenton sludge as an iron source for NiFe2O4 synthesis and its application in the Fenton-based process. J. Environ. Sci. **53**, 1–8 (2017). https://doi.org/10.1016/J.JES.2016.05.010

86. Bayram, T.; Bucak, S.; Ozturk, D.: BR13 dye removal using sodium dodecyl sulfate modified montmorillonite: equilibrium, thermodynamic, kinetic and reusability studies. Chem. Eng. Process. Process Intensif. **158**, 108186 (2020). https://doi.org/10.1016/j.cep.2020.108186

87. Katsumata, H.; Koike, S.; Kaneco, S.; Suzuki, T.; Ohta, K.: Degradation of Reactive Yellow 86 with photo-Fenton process driven by solar light. J. Environ. Sci. **22**, 1455–1461 (2010). https://doi.org/10.1016/S1001-0742(09)60275-8

88. Liu, H.; Li, G.; Qu, J.; Liu, H.: Degradation of azo dye Acid Orange 7 in water by Fe0/granular activated carbon system in the presence of ultrasound. J. Hazard. Mater. **144**, 180–186 (2007). https://doi.org/10.1016/J.JHAZMAT.2006.10.009

89. Hsueh, C.C.; Chen, B.Y.; Yen, C.Y.: Understanding effects of chemical structure on azo dye decolorization characteristics by Aeromonas hydrophila. J. Hazard. Mater. **167**, 995–1001 (2009). https://doi.org/10.1016/J.JHAZMAT.2009.01.077

90. Singh, S.K.; Tang, W.Z.; Tachiev, G.: Fenton treatment of landfill leachate under different COD loading factors. Waste Manag. **33**, 2116–2122 (2013). https://doi.org/10.1016/j.wasman.2013.06.019

91. Asghar, A.; Abdul Raman, A.A.; Daud, W.M.A.W.: Sequential optimization for minimizing material cost and treatment time of fenton oxidation for textile wastewater treatment. Chem. Eng. Commun. **204**, 873–883 (2017). https://doi.org/10.1080/00986445.2017.1320283

92. Pliego, G.; Zazo, J.A.; Casas, J.A.; Rodriguez, J.J.: Case study of the application of Fenton process to highly polluted wastewater from power plant. J. Hazard. Mater. **252–253**, 180–185 (2013). https://doi.org/10.1016/j.jhazmat.2013.02.042